University of Alberta

Study of Animal Movement and Group Formation with a Lagrangian Model

by

Rita Wong

A thesis submitted to the Faculty of Graduate Studies and Research
in partial fulfillment of the requirements for the degree of

Master of Science
in
Applied Mathematics

Department of Mathematical and Statistical Sciences

Spring 2011
Edmonton, Alberta

Examining Committee

Gerda de Vries, Mathematical and Statistical Sciences

Kelvin Jones, Phys. Ed. and Recreation
Adriana Dawes, Mathematical and Statistical Sciences
Mark Lewis, Mathematical and Statistical Sciences

To my parents.

Abstract

Animal group formation has often been studied by mathematical biologists through PDE models, producing classical results like traveling and stationary waves. Recently, Eftimie et al. introduced a 1-D PDE model that considers three social interactions between individuals in the relevant neighborhoods, specifically repulsion, alignment, and attraction. It takes into account the orientation of the neighbors when considering if they can communicate. This has resulted in exciting new movement behaviors like zig-zag pulses, breathers, and feathers. In this work, we translate the Eftimie model into a Lagrangian implementation. Currently, the results from the Lagrangian formulations show many of the results displayed by Eftimie's original PDE model, producing patterns like the zig-zag, breather traveling, and stationary pulses. In addition, we model animal movement with an ODE approach to complete the investigation regarding the role of direction-dependent communication mechanism in discrete-space. This implementation generates patterns like traveling breathers, traveling trains, and stationary pulses. Finally, we explore what types of patterns the Lagrangian model would generate if repulsion was prioritized. We discover that the sizes of the interaction ranges are significant in determining whether stationary, semi-zig-zag, zig-zag, or traveling pulses are formed. For all three model implementations, we find that the incorporation of direction-dependent communication enriches the model behavior.

Acknowledgements

I would like to thank my supervisor, Professor Gerda de Vries, for all her help in the past two years. Not only did she help me develop the research in this thesis, she also taught me how to be a better student by teaching me how to present my ideas clearly, written and orally. I would also like to acknowledge Raluca Eftimie for the idea of the animal movement model and Cole Zmurchok for his assistance with the Eftimie-Kolpas hybrid.

I appreciate very much the funding from the University of Alberta Graduate Recruitment (2009) and NSERC CGS-M scholarships (2010).

I would also like to thank my parents for their patience, generosity, and unconditional support. They helped me get through the difficult times during the last two years.

Table of Contents

List of Tables

List of Figures

List of Symbols

Chapter 1

Introduction

1.1 Overview

Social organization is a topic of interest for mathematical biologists because group formation is an important survival skill for certain animals. For example, for simpler animals like fish, where there are no group leaders, schooling provides benefits like protection from predators and efficiency in catching prey ([9], [10], [11]).

When considering how animals interact, it is important as a modeler to determine the crucial interaction forces. A large class of movement models focuses on three interaction forces, namely attraction, alignment, and repulsion, as shown in Figure 1.1 ([4], [14], [17], [22], [25], [26]). Typically, repulsion is assumed to act over a short distance from the reference individual. In the repulsion zone, the individuals would turn away from adjacent neighbors to avoid collision. Attraction occurs primarily between neighbors from a farther neighborhood to ensure that animals can still form groups. It is usually assumed that alignment acts in an intermediate area located between the repulsion and attraction zones. While many models include repulsion, alignment, and attraction forces between neighbors, some choose to ignore alignment.

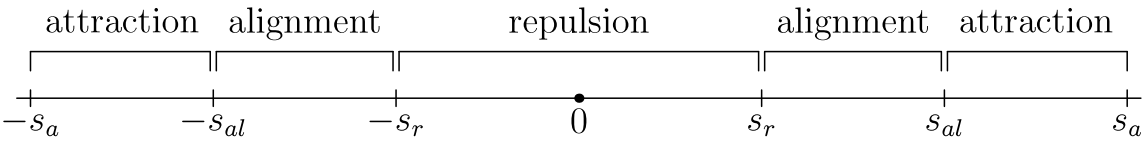

Figure 1.1: Illustration of the interaction zones. A reference individual is repulsed by the neighbors who are in the region immediately adjacent to it. It tends to align with those who are in an intermediate range and is attracted by those who are in a farther range. The parameters $s_{r,al,a}$ are the limits of the interaction zones.

For self-organizing animals like fish, there are two general modeling approaches: Lagrangian and Eulerian. The main difference is that the Lagrangian approach is at an individual level, while the Eulerian approach is at a population level. The Lagrangian formulation tracks individuals and follows their paths, and the Eulerian formulation examines a fixed location and the amount of traffic passing through ([24]).

Because the Lagrangian approach focuses on the individual and the decision-making process, it is useful for simulating animal behavior and making predictions. For example, biological experiments can motivate hypotheses that attempt to explain how animals congregate, and these predictions can easily be tested by the mathematical model. Also, Lagrangian formulations provide a fast, convenient way to explore the parameter space ([12]). Since the numerical simulations are modeled from a reference individual's view, the significance of each parameter is intuitive ([28]). The main disadvantage is that there are no analytical solutions. Thus, there is usually no gain of theoretical insight as to why the interactions result in the observed behavior. In addition, the simulations can be computationally expensive.

One of the benefits of using a Lagrangian formulation is to simulate the model and provide visualizations. Some researchers may use a property like the average distance from the closest neighbor for statistical analysis purposes ([18]). Essentially, Lagrangian models can only provide an answer as to what a particular parameter set and initial condition would generate, but one cannot show decisively with any mathematical theory how the behavior may change according to each parameter. While the Lagrangian framework is useful for determining which properties are crucial for building a suitable mathematical model, it must be translated into an Eulerian model for rigorous mathematical analysis.

In contrast, the Eulerian approach allows for the application of established mathematical ideas, like bifurcation theory. It is easier to compare results from different Eulerian models, as they are often more mathematically rigorous and can therefore be described quantitatively rather than qualitatively. Because there are many mathematicians interested in this area, there are many references available and a number of formulas for certain well known partial differential equation systems. In addition, even if the system is too complicated to have an explicit solution, one can often find the steady-state or equilibrium state.

In this thesis, we model animal movement using assumptions from the Eftimie model ([9], [10], [11]). The reason why we work with this model is because it introduced an exciting new idea: direction-dependent communication. The incorporation of this element in the Eftimie PDE model led to many new aggregation patterns. Interestingly, these communication rules have never been used in a Lagrangian implementation before. Therefore, we would like to investigate a Lagrangian movement model using these assumptions from the Eftime model and see if any new patterns can be found.

In Section 1.2, we will review Lagrangian movement models and examine the different aspects of animal

motion that can be incorporated into a Lagrangian formulation. In Section 1.3, Eulerian movement models are reviewed briefly to explain why they are useful in studying pattern formation. In Section 1.4, we formulate the questions we would like to investigate in this project. Finally, in Section 1.5, we outline the chapters in the thesis and discuss the objectives of this project.

1.2 The Development of Lagrangian Movement Models

The mechanism of animal group formation has been studied extensively. There are a few common traits that can be found amongst most of these models. The underlying assumption in the Lagrangian models discussed below is that one or more local interaction forces between the reference individual and its neighbors produce a global pattern throughout the population. In general, the closest neighbors produce a repulsion force and the farthest neighbors result in an attractive force. Alignment is also considered in some models. Depending on how these forces are calculated, different Lagrangian models can produce a range of aggregation patterns formed by simple animals, like birds and fish. It is important to establish a thorough understanding of the development in modeling animal movement from the Lagrangian perspective. Therefore, in this section, we will be discussing several important movement models that have introduced new ideas in the field.

1.2.1 The Huth and Wissel Model

In 1992, Huth and Wissel ([16]) formulated a Lagrangian model in two-dimensional space describing how fish schools aggregate with the consideration of three interaction zones. Fish are an ideal choice for modeling group formation because they have been shown to swim in groups without external influences from any prey or predator. The set-up of the interaction zones is similar to that described in Figure 1.1 except the zones are now in the shape of concentric circles because of the additional spatial dimension. There is a "blind" area behind each individual where no neighbor is detected. In addition, only a fixed number of neighbors is considered when determining the turning probability. With these assumptions, the model establishes that fish can aggregate in two different types of structures: a tightly knit group with very high polarization and a loosely gathered group with low polarization.

1.2.2 The Couzin Model

While the Huth and Wissel model can be thought of as a simplified, two-dimensional version of an animal movement model without directional dependence, the Lagrangian model of Couzin *et al*. ([4]) is much more complicated by incorporating inhomogeneities in the individuals traveling in three-dimensional space.

Again, the three interactions considered are repulsion, alignment, and attraction, but in this model, repulsion is the most important consideration to avoid collisions. When animals are present in the repulsion zone, alignment and attraction are ignored when considering the turning probability. The behavior of the group is described by two vectors, $\vec{c}$ and $\vec{v}$, which store respectively the location and velocity of every individual. All the neighbor's influences on the reference individual are first calculated, and then the subsequent velocity of the reference individual is determined according to these influences. The surroundings of an individual is divided into interaction zones as in Figure 1.1 except the zones are now in the shape of spheres.

The two model variables are c_i and v_i, which respectively keep track of the location and velocity of the i^{th} individual. τ is an independent variable designating the constant time step. To calculate the turning probability of each animal, Couzin *et al.* introduce three new terms, $d_{r,al,a}$, where d is the influence from surrounding neighbors and the subscript refers to the type of communication mechanism involved. Repulsion is denoted by the subscript r, alignment by al, and attraction by a. The values $n_{r,al,a}$ define the limits of the repulsion, alignment, and attraction zones. The model uses the following equations, which are of a common form that is found in many Lagrangian animal movement models:

$$\vec{d_r}(t+\tau) = -\sum_{j\neq i}^{n_r} \frac{\vec{r}_{ij}(t)}{|\vec{r}_{ij}(t)|}, \tag{1.1}$$

$$\vec{d_{al}}(t+\tau) = \sum_{j=1}^{n_o} \frac{\vec{v}_j(t)}{|\vec{v}_j(t)|}, \tag{1.2}$$

$$\vec{d_a}(t+\tau) = \sum_{j=1}^{n_a} \frac{\vec{r}_{ij}(t)}{|\vec{r}_{ij}(t)|}, \tag{1.3}$$

$$\tag{1.4}$$

where

$$\vec{r}_{ij} = \frac{(\vec{c}_j - \vec{c}_i)}{|(\vec{c}_j - \vec{c}_i)|}. \tag{1.5}$$

Equation (1.1) essentially sums the relative positions of the neighbors in the repulsion zone and directs the reference individual away from this direction, while equation (1.3) does the exact opposite by directing the reference individual towards the sum of the relative positions of the neighbors in the attraction zone. Equation (1.2) determines the net orientation of the neighbors in the alignment zone and turns the individual in that particular direction.

If there are any individuals in the repulsion zone, then equations (1.2) and (1.3) are not used and the new direction is given by:

$$\vec{v}_i(t+\tau) = \vec{d_r}(t+\tau). \tag{1.6}$$

Given the case where there is no repulsion and only attraction and alignment, the new direction after a time step is given by:

$$\vec{v}_i(t+\tau) = \frac{1}{2}(\vec{d}_o + \vec{d}_a). \tag{1.7}$$

The model also has the feature of restricting the animal to a maximum turning angle. If the angle between $\vec{d}(t+\tau)$ and $\vec{d}(t)$ is greater than this limit, then the animal only turns the maximum angle towards $\vec{d}(t+\tau)$ instead of simply using the vector as its new direction.

With this formulation, Couzin *et al*. observed four types of patterns: swarm, torus, dynamic parallel group, and highly parallel group. A swarm is where the individuals aggregate in a condensed region with low polarization. A torus is where the individuals continually rotate around an empty domain. Both dynamic and highly parallel groups are structures where the individuals move in one direction collectively. However, in the dynamic parallel group, the individuals are much more likely to exchange positions within the internal structure than in the highly parallel group.

In comparison to the model of Huth and Wissel, an additional feature that the Couzin model explores is the dependence of group formation on the present pattern. In other words, the initial conditions can affect how the group transitions into different behaviors as the individual interactions change. This discovery shows that animal movement and group formation does, in fact, take into account previous patterns and collective memory plays an important role.

1.2.3 The Gueron Model

Although most of the Lagrangian models assume constant speeds, this may not always be the case. Gueron *et al*. ([14]) studied the transition from separately traveling individuals to aggregated groups with the assumption that speed can vary. This is achieved by the incorporation of speeders, a subgroup that travels faster than the rest, leaders, animals at the front who tend to slow down and wait for those behind them, and trailers, animals in the rear zone who can speed up to catch up. In this particular two-dimensional model, repulsion and attraction act on a short and long range respectively. The repulsion and attraction zones are separated by a neutral territory, where no social interaction is considered. The authors conclude that the probability of fragmentation increases with the level of inhomogeneity. Most importantly, the authors find that with this movement model, there is an optimal size for the neutral zone where animals can simply travel at a constant speed and maintain a coherent group structure without acceleration or deceleration, allowing them to conserve energy.

1.2.4 The Kolpas Model

Kolpas' model describes animals moving on a 1-D lattice ([18]). It is important to discuss the Kolpas model in detail as an example because its framework is similar to many Lagrangian 1-D movement models. Its pseudocode is also useful because the general set-up can be applied to variations of animal networks that communicate with different mechanisms. A variation of this pseudocode is used in this project, and this discussion will be further continued in Chapter 3 after other components of the project are introduced.

In the Kolpas model, the velocity is ± 1. There are three distinct zones where neighbors exert a repulsion, alignment, or attraction force. There is no interaction kernel, since all neighbors in the relevant neighborhoods are assumed to have the same effect on the reference individual. In the repulsion zone, the average of all the neighbors' relative position is calculated.

$$V = -\sum_{c_j(t) \in Z_{r_j}(t)} \frac{c_j(t) - c_i(t)}{|c_j(t) - c_i(t)|}, \tag{1.8}$$

where $c_i(t)$ is the position of the i^{th} individual at time t, $v_i(t)$ is the velocity of the i^{th} individual at time t, and $Z_{r_j}(t)$ is the repulsion zone for the j^{th} individual. It is a priority for the reference individual to orient itself away from its adjacent neighbors according to the above equation to avoid any collisions. Therefore, it is of emphasis that equation (1.8) is the only equation used for calculating the new velocity if there are individuals present in the repulsion zone. In other words, the model no longer considers alignment and attraction as an effective interaction force for an individual who senses neighbors in its repulsion zone. The non-zero value given by equation (1.8) is then normalized according to equation (1.10), which is given below.

If there are no neighbors in the repulsion zone, the individual would tend to follow the average direction of the neighbors in the alignment zone and move towards the neighbors in the attraction zone. In other words, the following equation for calculating velocity will only be relevant if equation (1.8) is not applicable. Both these influences affect the reference individual's turning probability equally, as shown by the following equation where the two are averaged to determine the net effect.

$$V = \frac{v_i(t) + \sum_{c_j(t) \in Z_{o_j}(t)} v_j(t)}{|v_i(t) + \sum_{c_j(t) \in Z_{o_j}(t)} v_j(t)|} + \sum_{c_j(t) \in Z_{a_j}(t)} \frac{c_j(t) - c_i(t)}{|c_j(t) - c_i(t)|}, \tag{1.9}$$

where $Z_{o_j}(t)$ and $Z_{a_j}(t)$ are the alignment and attraction zones of the j^{th} individual respectively. If V is determined to be zero, this means that the attraction and alignment effects cancel out each other and the individual continues in the previous direction. Otherwise, V is normalized and used as the velocity for the

following time step:

$$\tilde{v} = \begin{cases} v_i(t), & V = 0, \\ \frac{V}{|V|}, & \text{otherwise}, \end{cases} \tag{1.10}$$

where $v_i(t)$ is the current velocity.

Finally, stochasticity is incorporated with the parameter p, $0 < p < 1$. p is the probability that an individual changes its direction randomly.

$$v_i(t+1) = \begin{cases} -\tilde{v}, & X < p, \\ \tilde{v}, & \text{otherwise}, \end{cases} \tag{1.11}$$

where $v_i(t+1)$ is the velocity at the following time step and X is a uniform random variable between 0 and 1.

The initial position and velocity vectors are chosen randomly, and the simulations are run until a steady state emerges. At each step, the interactions from the neighbors are calculated according to the given equations.

The pseudocode of the Kolpas model is given by the following scheme:

1. Create a finite 1-D lattice with the spacing defined by the animal's step size.
2. Distribute the total number of individuals over the lattice and assign directions to them randomly.
3. For each individual, scan its repulsion zone. If it is empty, skip to step 4. Otherwise, determine whether or not the animal would turn according to equation (1.8). If yes, negate the direction and skip to step 5.
4. If the repulsion zone is empty, scan the alignment and attraction zones and use equation (1.9) to determine whether the animal should turn. If yes, negate the direction.
5. Use equation (1.11) to determine whether or not the animal will turn simply due to stochasticity.
6. Repeat steps 3-5 for all the individuals.
7. Let the animals move one step along the lattice according to their directions.
8. Repeat step 3-7 until the animals have completed the designated number of steps.

With the above mechanism, the Kolpas model has been able to produce stationary and traveling pulses. In fact, the animals transition between the two behaviors are simply due to stochastic effects, which is a result not seen in any previous discussed models. The steps used by Kolpas *et al*. will be discussed again in Chapters 3 and 5, for the purposes of simulating another animal movement model.

1.2.5 Models from a Physics Point of View

The Lagrangian formulation is not only limited to discrete velocities and locations. For example, many models use Newton's second law of motion to describe a particle's trajectory under the imposed forces. For example, Levin *et al*. [20] use the following system of equations to describe a system of N self-propelled, interacting particles:

$$m_i \partial_t \vec{v}_i = \alpha \hat{f}_i - \beta \vec{v}_i - \partial_{\vec{x}} U, \tag{1.12}$$

$$\partial_t \vec{x}_i = \vec{v}_i, \tag{1.13}$$

where each particle is defined by mass m_i, position $\vec{x}_i$, and velocity $\vec{v}_i$. Furthermore, each particle is driven by a self-propelling force with fixed magnitude α and hindered by a friction force with coefficient β. The interaction function U characterizes a communication mechanism where each particle is under the influence of its neighbors via two forces, a long-range attraction force limited by the interaction range l_a and a short-range repulsion force limited by the interaction range l_r. Like the discrete velocity models above, the interaction terms are incorporated into U in the following form:

$$U = \sum_{j \neq i} C_a \exp\left(\frac{|\vec{v}_i - \vec{v}_j|}{l_a}\right) - \sum_{j \neq i} C_r \exp\left(\frac{|\vec{v}_i - \vec{v}_j|}{l_r}\right). \tag{1.14}$$

For the movement models with Newton's second law as a basis, the general form of the equations describing the displacement and velocity do not change. However, by varying the forces the particles are subject to, different results can be obtained. In fact, some analytical results may be obtained if the interactions functions are of a simple form. In particular, existence conditions have been derived for perfect schools and mills ([21], [30]). The perfect school refers to an aggregation where all the inter-particle distances and speeds are identical. For example, fish display this type of formation. The perfect mill is a group pattern where particles travel behind one another in a closed circle equally spaced from one another. This implies that the group has a constant angular velocity, circle radius, and inter-particle spacing. For example, Li *et al*. [30] discuss a model that deals with perfect schools. In this model, only repulsion and attraction between the reference individual and its closest neighbor are considered. This simplification is necessary to find the existence condition analytically and prove that only local interactions depending on inter-distance are required to form a perfect school.

The mechanism by which birds form perfect groups has also been explored by Cucker *et al*., but without the incorporation of Newton's second law ([6]). Instead, the modelers track how the energy of the flock

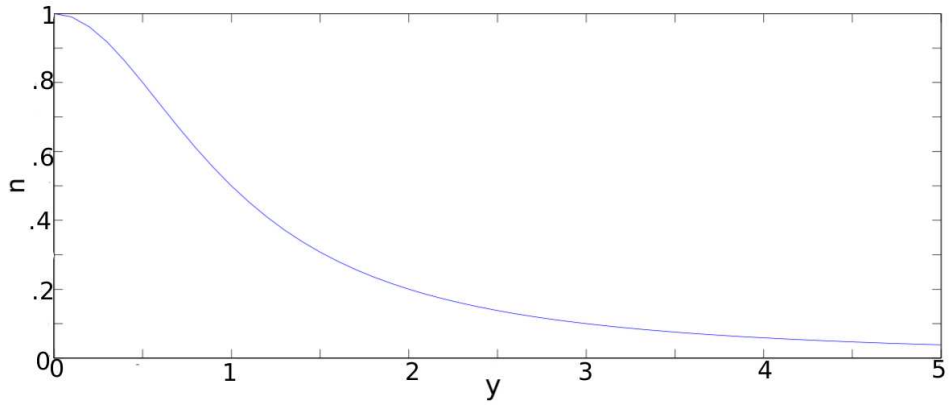

Figure 1.2: Scaling factor for the alignment force ($\eta(y)$). This is a sample plot to show that the alignment force decreases as y, the distance between reference individual and the neighbor, increases. Parameters: $K = 1, \sigma = 1, \beta = 2$.

varies according to the configuration. The equations governing motion are given by the following:

$$v_i(t+1) - v_i(t) = \sum_{j=1}^{k} a_{ij}(v_j(t) - v_i(t)), \tag{1.15}$$

$$a_{ij} = \eta(\| x_i - x_j \|^2), \tag{1.16}$$

$$\eta(y) = \frac{K}{(\sigma^2 + y)^\beta}. \tag{1.17}$$

The above system of equation considers a total of k birds, each possessing a velocity described by v_i and $i = 1, ..., k$. Equation (1.16) specifies the scaling factor for the alignment force given by equation (1.15) depending on the relative distance between the reference individual and the neighbor. There are several important properties of η, the function specified in equation (1.17) used for calculating this scaling factor. It is positive and non-increasing. The parameters K and σ define the location and value of the maximum of η, and β is the decay rate of the alignment signal.

The only interaction force considered is the alignment force, and the bird's velocity changes according to the difference between its own velocity and those of its neighbors. Interestingly, with the distance-dependent function η (see Figure 1.2), Cucker *et al*. found that the emergence of a perfect flock with uniform velocity depends on the parameter β. When β is sufficiently small, a perfect flock is guaranteed under any initial conditions. When β becomes too large, a perfect flock will only emerge under certain initial conditions.

Again using a physics perspective, the Lukeman *et al*. model ([21]) studies milling formations with only short-range repulsion and long-range attraction. The most interesting aspect of this paper is that it derives

analytically the form of the schooling force, which depends on the inter-particle distance:

$$\vec{f_i} = g(|\vec{x}_j - \vec{x}_i|)\frac{(\vec{x}_j - \vec{x}_i)}{|\vec{x}_j - \vec{x}_i|}, \tag{1.18}$$

where j indicates the closest neighbor to the reference individual. The existence condition for the perfect mill is that the interaction function g must satisfy the following:

$$g(d) = sd, \tag{1.19}$$

$$s = \frac{\gamma^2}{2} cos^2(\frac{\pi}{n}). \tag{1.20}$$

where s is a function of γ and n, which represent the drag coefficient and the population size respectively. While some previous models have also been able to generate milling formations, the Lukeman model considers a more general form of the interactions.

Given very simple interaction functions, some Lagrangian models have been able to produce some analytical results. However, for a more complex system, to decisively determine the effects of each parameter on the system and look for steady-state solutions, a Lagrangian system must still be translated into an Eulerian model for analysis purposes. In the Eulerian model, instead of tracking the velocity and location of the individual, the system examines the averaged behavior of the entire system. Depending on the purpose of the model, either a Lagrangian or an Eulerian model may be used.

1.3 Some Eulerian Movement Models and their Results

Because no rigorous proofs can be deduced from a Lagrangian model, a Lagrangian model is often translated into an Eulerian model for the application of mathematical analytical techniques by using approximations. Often, a set of PDE equations are derived from master equations which describe how the individuals interact and travel collectively. Many movement models, like the Mogilner *et al*. model ([23]), use a one-dimensional advection-diffusion equation to describe the geometries a swarm can exhibit ([5]). The population density, f, is described by the following equation:

$$\frac{\partial f}{\partial t} = \frac{\partial}{\partial x}(D\frac{\partial f}{\partial x} - Vf), \tag{1.21}$$

where x is the spatial coordinate, t is the time, D is the diffusion coefficient, and V is a drift term accounting for velocity changes from social interactions, namely short-range repulsion and long-range attraction. The results only show swarming behavior with constant interior density and sharp profiles. More factors can be incorporated to this basic form. For example, D may be a function of the population density instead of a constant parameter.

If factors like birth, death, emigration, and immigration are ignored, then the following population conversation equation must also be obeyed:

$$f_t + \bigtriangledown \cdot (\vec{v} f) = 0, \tag{1.22}$$

where $\vec{v}$ is the velocity vector. Similar to the Lagrangian formulation, this vector has two components: aggregation, $\vec{v}_a$ and dispersal $\vec{v}_d$:

$$\vec{v} = \vec{v}_a + \vec{v}_d. \tag{1.23}$$

Depending on how $\vec{v}_a$ and $\vec{v}_d$ are calculated, different group patterns can be obtained.

The general form of equation (1.21) is not only limited to the description of animal movement but also microscopic organisms like bacteria as well. However, in most of these systems, there is a growth term instead of a drift term because bacteria reproduce much more quickly than animals. A well-known example is the Fisher-Kolmogorov equation, which satisfies the following form:

$$\frac{\partial u}{\partial t} = D \bigtriangledown^2 u + f(u), \tag{1.24}$$

where $f(u)$ is a reaction function and u is the population fraction. In the case of the Fisher-Kolmogorov equation, $f(u)$ is a growth term written as:

$$f(u) = u(1 - u). \tag{1.25}$$

Similar to the animal movement models, there can be communication incorporated into a system describing a bacterial colony too. For example, the bacteria may release attraction or repulsion signals to each other by secreting chemicals ([2]).

One trait that these PDE models share is that they do not display a wide variety of behaviors. They usually only show one type of behavior. For example, most PDE models, including the previous one mentioned, only support swarms, either traveling or stationary. Often, for these PDE models, it is difficult to decide on a set of realistic interaction rules that would generate biologically relevant results. The difficulty arises from the fact that traveling groups of animals show sharp profiles at the front and the back ([7], [23]). In contrast, for the Eftimie model, which will be discussed in more detail, there is a wide range of results due to the flexibility from choosing the communication mechanisms ([9], [10], [11]). The stationary pulses can also exhibit uniform interior density and sharp edges or contain interior subgroups where the population density is higher.

In [9], [10], and [11], Eftimie *et al*. developed a 1-D Eulerian model for animal grouping. This model is applicable for simple animals without a hierarchy or influences from any predator or prey, like fish and

insects. The Eftimie model only considers neighbors with a particular direction for each social interaction, and this additional feature has allowed many new movement models. This is particularly interesting because previous models were only able to show congregation behavior. No complex patterns could be found, even when more factors are considered like movement in higher dimensions, hierarchal structures in the animal groups, and an ability to change velocity ([1], [4], [18], [29]). In fact, they have only produced stationary and traveling pulses, meaning that the animals are congregated in one or more groups either being stationary or traveling in a single direction. In contrast, the Eftimie model is able to produce two types of stationary pulses, one with uniform interior density and sharp edges or one with interior subgroups where the population density is higher ([9], [10], and [11]). The fact that a larger range of results is available is due to the flexibility in choosing the communication mechanisms. It should be emphasized that the primary distinguishing factor between the Eftimie model and the previous models mentioned is that direction dependent animal communication is now considered.

1.4 Statement of Problem

The Eftimie model, by introducing direction-dependent animal communication, has expanded the range of patterns observed with Eulerian models, which have only been able to show behavior like traveling and stationary pulses and, in some cases, vortices. The new behaviors include patterns like breathers and zig-zag patterns. A zig-zag pulse is formed when animals travel and spontaneously switch directions together. A breather pulse is similar to a stationary pulse, but the animals continually move away from the centre of the pulse and then return. These new patterns demonstrate that the formulation of this model is more general and hence more appropriate to model the movement of a larger set of simple animals. Therefore, it is important to confirm the results of the model and further explore other variations of this general framework to seek new patterns.

Having established the benefits of the general framework of the Eftimie model, the logical question to ask is: will the results produced by the Eulerian model at the population level be reflected by a model on an individual level? Will the new behaviors still be present when the direction-wise communication rules are applied to each individual animal in the system? A translation into a Lagrangian formulation would help answer these questions. By doing this, we are verifying that the individual behavior does, in fact, reflect the conclusion reached by the mean field approximation.

The current goal is to use the assumptions of the Eftimie model in a Lagrangian formulation in a discrete-space and discrete-time system to see if the analytical results obtained for the Eftimie model can be repli-

cated. The motivation for building an individual-based model with the same assumptions is to provide a more convenient framework for incorporating both deterministic and stochastic factors and an easier, faster way to simulate animal motion. Also, any additional approximations when the master equations are transformed into partial differential equations would be avoided. These are common benefits of the Lagrangian approach, as it is more focused on the individual level rather than the population level ([28]). The main problem is to determine the parameter space for which the Lagrangian model would generate similar results to the Eulerian model and if all the patterns from the analytical results are obtainable from the computer simulations. If there are significant differences between the results of the Eulerian and Lagrangian model, then what is the reason?

As a further exploration of direction-dependent communication in Lagrangian models, we apply the same communication rules from the Eftimie model into the Kolpas model. The Kolpas model mainly differs from the Eftimie model by assuming that animals prioritize repulsion over alignment and attraction over repulsion in order to prevent collisions. A question we investigate is how this emphasis on repulsion will affect the range of behaviors produced. Also, how will the sizes of the interaction zones influence the animal movement? By extending our research in Lagrangian models, we can compare the two different formulations, the Lagrangian Eftimie model and the Eftimie-Kolpas hybrid, and have a better insight of what factors are critical for animals to move collectively as a group.

In addition to a discrete-space and discrete-time system, it is also possible to keep track of the number of animals at each grid-point in continuous time by using a discrete-space, continuous-time formulation. This results in an ODE system with each equation keeping track of the population at a grid-point. Again, here the question is if results from the Eulerian model are available with this formulation. If so, given that a certain pattern is observed for both the Lagrangian systems, how would the parameters for the discrete-space and time system vary with respect to those of the ODE system? What causes this change? These are questions that will be addressed in this project in order to gain a better understanding the role of communication mechanisms in animal movement.

1.5 Thesis Outline

In Chapter 2, we give a review of the Eftimie model, for understanding the Eulerian model better allows us to build a more accurate individual-based version. Due to the benefit of being able to use established mathematical theory and determine bifurcation values and the dispersion relation, Eftimie *et al*. chose to use the Eulerian approach for modeling animal movement under the influence from neighbors in the relevant neigh-

borhoods. This is the suitable choice for finding mathematically rigorous conditions for pattern formation. We briefly discuss the useful analytical results that have been established.

However, an unanswered question is whether the approximations taken when deriving the PDE's from the master equations would alter the behavior of the model. Specifically, the objective of this project is to compare the results from the Eftimie model to those produced by a Lagrangian formulation. To achieve this, we use a Lagrangian approach to simulate pattern formation, which will be presented in the following chapters.

In Chapter 3, the Lagrangian model will be discussed in detail. We formulate an individual-based computational scheme that reflects the behavior and communication mechanism of animals that are described in the Eftimie model. Here, we find that this scheme can generate a large range of behaviors, some of which have never been found by previous Lagrangian models.

In Chapter 4, we focus on the question of how a system in discrete space and continuous time would be different from one with both time and space continuous or discrete. First, we use the method of lines to derive an ODE system from the Eftimie PDE model. It is very important to ensure that the spatial derivative discretization is numerically stable. The ODE system can be considered to be an intermediate between the Lagrangian and Eulerian formulations, since it has one continuous and one discrete continuous variable. The ODE model generates another set of aggregation patterns, but this set does not completely overlap with those of the Lagrangian or PDE formulation. This work would help identify how three different models that describe animals following the same set of interaction rules can generate different results, simply based on which independent variables, time and space, are continuous.

In Chapter 5, we incorporate Eftimie's direction-dependent communication mechanisms in the Kolpas model and implement two separate versions, one with interaction kernels and one without. A relationship is established between the sizes of the interaction zones and the aggregation behavior, and more patterns are generated with the hybrid model when compared to the original Kolpas model. Also, we find that some submodels do not display any aggregation behavior when both interaction kernels and direction-dependent communication are incorporated into the Kolpas model.

Finally, in Chapter 6, we compare and contrast the results and pattern range generated with the different formulations. The three different formulations effectively complete the set of possible continuous and discrete time and space systems that can be implemented, allowing us to thoroughly explore the movement mechanism proposed by Eftimie *et al*. in various settings. Because of the differences in the discretization of the variables, it is expected that not all patterns will be available in the Lagrangian and ODE models. In addition to discussing the implementations of the Eftimie model, we also discuss the behaviors and trends found

with the Eftimie-Kolpas model. Most importantly, we give examples of where these patterns are observed in nature and how these mathematical models have helped us further understand the role of communication signals in animal movement.

Chapter 2

Review of the Eftimie Model

2.1 Introduction

In this chapter, we discuss the formulation and results of the Eftimie model thoroughly, as it will serve as a foundation for our project. In Section 2.2, we review the derivation of the model from first principles to describe how the animals move in 1-D space as they change directions according to the influences of their neighbors. Then, in Section 2.3, we review the behavioral patterns generated by this PDE system.

2.2 Formulation of the Model

In the 1-D Eulerian model by Eftimie *et al*. ([9], [10], [11]), three social interactions, specifically repulsion, alignment, and attraction, are considered, and the animals are assumed to be moving at constant speed. Eftimie *et al*. included a direction dependence when considering which neighbors contribute to each social interaction ([9], [10], [11]). This dependence gives rise to many submodels (see Figure 2.1). Submodels differ from each other in which set of neighbors is involved in determining whether the reference individual turns or not. For example, the most general submodel, submodel M2, would consider all neighbors for every social interaction, while a modification, submodel M3, would be where the individuals only sense the neighbors ahead of them.

According to the Eulerian model by Eftimie *et al*. , the following system of partial differential equations can be used to describe an animal group split into two different subgroups defined by their directions of movement, where $u^{\pm}(x,t)$ is the number of right-moving (+) and left-moving (-) individuals at location x

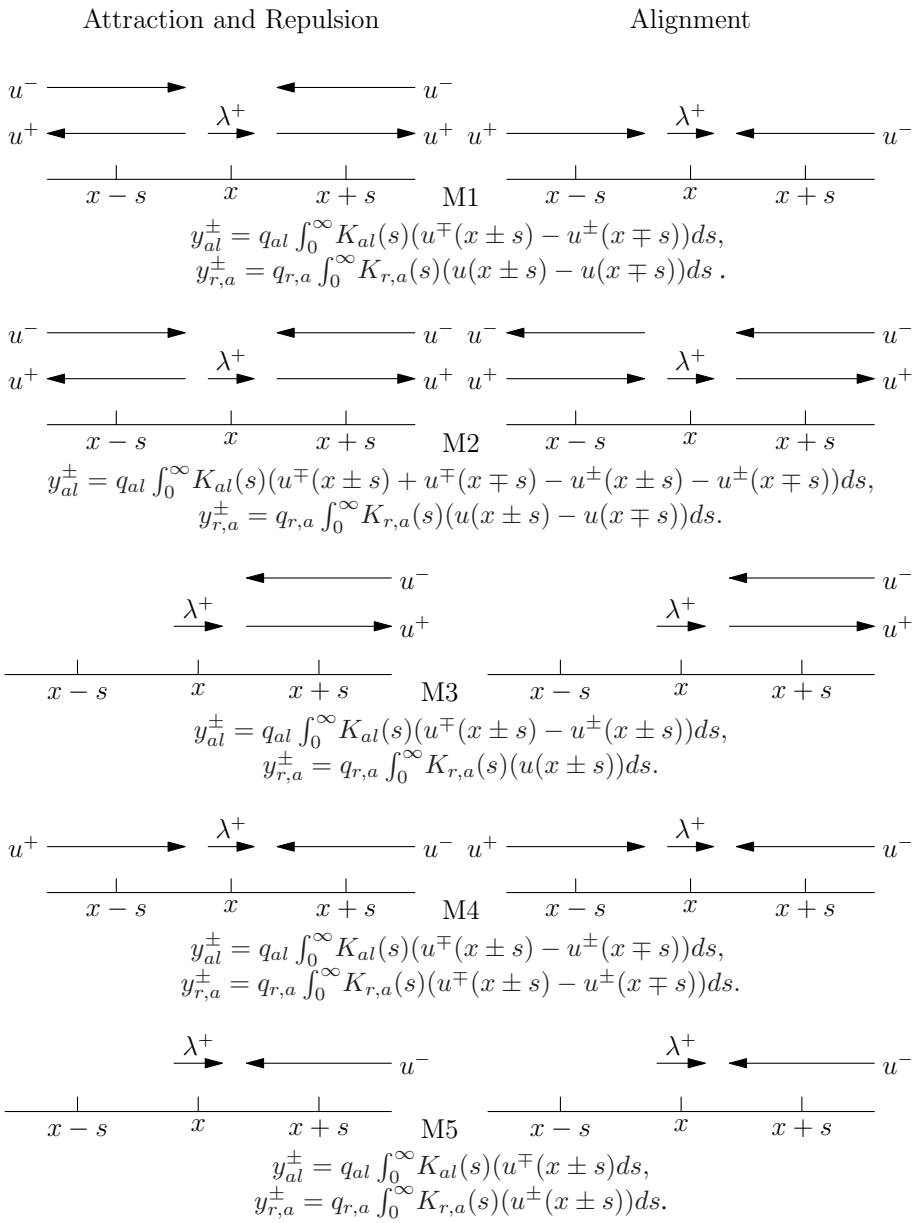

Figure 2.1: Description of submodels. The above figures summarize the interaction rules by right-moving individuals for all five submodels considered in the Eftimie model. For example, in submodel M1, attraction and repulsion consider all neighbors in the relevant zones, while alignment only takes into account those that are moving towards the individuals.

at time t, and $\lambda^{\pm}$ is the probability of a right (left)-moving individual to switch direction:

$$u_t^+(x,t) + \gamma u_x^+(x,t) = -\lambda^+ u^+(x,t) + \lambda^- u^-(x,t), \tag{2.1}$$

$$u_t^-(x,t) - \gamma u_x^-(x,t) = \lambda^+ u^+(x,t) - \lambda^- u^-(x,t), \tag{2.2}$$

where γ is the constant speed of the individual.

In the Eulerian model, the total turning probabilities are given by the following functions ([9], [10], [11]):

$$\lambda^{\pm}(y_r^{\pm} - y_a^{\pm} + y_{al}^{\pm}) = \frac{\lambda_1}{2} + \frac{\lambda_2 f(y_r^{\pm} - y_a^{\pm} + y_{al}^{\pm})}{2}, \tag{2.3}$$

$$f(y_r^{\pm} - y_a^{\pm} + y_{al}^{\pm}) = 0.5 + 0.5\tanh(y_r^{\pm} - y_a^{\pm} + y_{al}^{\pm} - y_0), \tag{2.4}$$

where λ_1 is a random turning probability and $\lambda_2 f$ is a turning probability as a function of interactions with neighbors. The functionals $y_i^{\pm}[u^+, u^-]$ represent repulsion, attraction, and alignment signals from neighbors that determine the turning rate, and r, a, al denote repulsion, attraction, and alignment respectively. y_0 is a constant chosen such that f is small when the input is small. Equation (2.4) has two important properties. First, it is positive and non-decreasing. Second, f is close to zero when the signals are very low and close to one when they are strong. We would like to emphasize that f is not restricted to the form shown in equation (2.4). In fact, any function satisfying the two properties is a possible candidate for calculating the turning probability.

Signals from neighbors to the left and to the right are received and processed by the individual to decide whether to turn or not (see Figure 2.1). Depending on the particular submodel and the criterion for the neighbor to be detected, there are many variations for the equations describing signal strength considered by Eftimie *et al.* , five of which are shown in Figure 2.1. The equations can be inferred from the accompanying figures describing how the individuals interact in each submodel.

The following is the set of equations for right-moving individuals that are of interest, expanded from the description of submodel M1 in Figure 2.1:

$$y_{al}^+ = q_{al}\int_0^{\infty} K_{al}(s)(u^-(x+s) - u^+(x-s))ds, \tag{2.5}$$

$$y_r^+ = q_r\int_0^{\infty} K_r(s)(u(x+s) - u(x-s))ds, \tag{2.6}$$

$$y_a^+ = q_a\int_0^{\infty} K_a(s)(u(x+s) - u(x-s))ds, \tag{2.7}$$

where $u = u^+ + u^-$. The $K_i(s)$ are interaction kernels (discussed below), and q_i indicates the strength of the social interaction's influence.

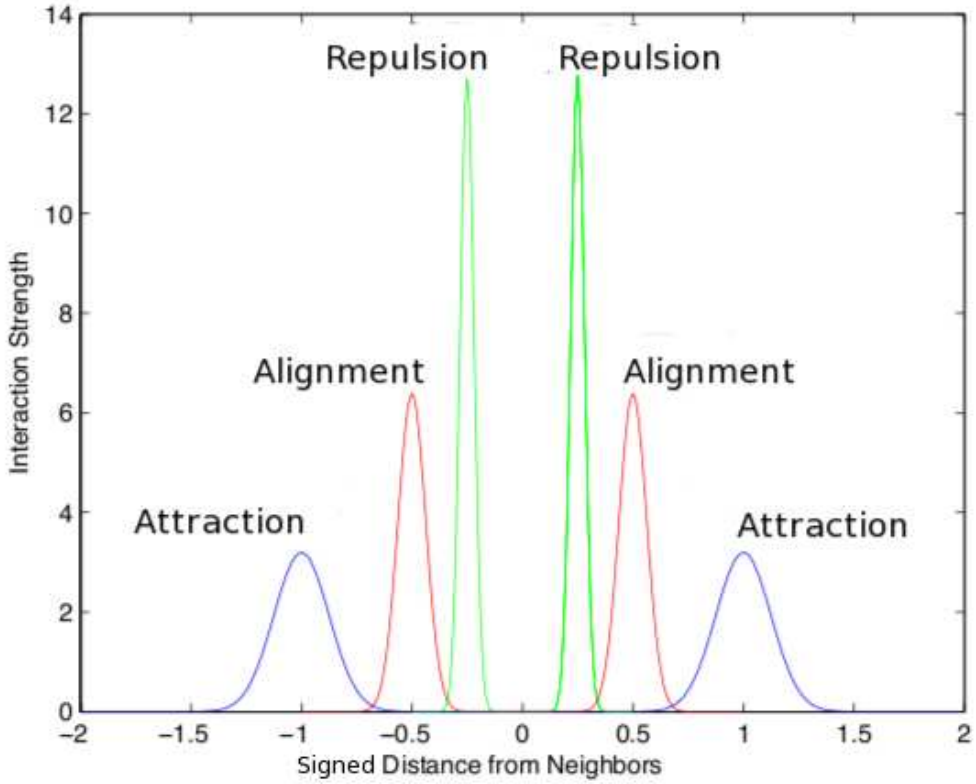

Figure 2.2: Gaussian interaction kernels from the Eftimie Eulerian model.

In the continuous-space Eulerian model, the strength of the interaction signal from a neighbor is determined by the interaction kernel, defined by a translated Gaussian function (see Figure 2.2):

$$K_i(s) = \frac{1}{\sqrt{2\pi m_i^2}} \exp(\frac{-(|s| - s_i)^2}{2m_i^2}), s \in [-\infty, \infty), \tag{2.8}$$

where s is the distance between an individual and its neighbor, m_i is width of interaction zone, and s_i is distance between the peak of the interaction kernel and the individual. Because of the underlying assumptions of the repulsion, alignment, and attraction zones (see Figure 1.1), s_r is the smallest, and s_a is the largest. Using the above formulation, the Eulerian model can produce a wide variety of different behaviors. It is reasonable to expect similar behaviors in the discrete-space, discrete-time system.

A closer look at the formulation of y_{al} and $y_{r,a}$ for each submodel would show that the equations them-

selves are a reflection of how these animals impact each other's directions of motion. For every set of equations described in Figure 2.1, the following factors are involved: $q_{r,a,al}$ and $K_{r,a,al}$, where $q_{r,al,a}$ are the strengths of the interaction signals and $K_{r,al,a}$ are the interaction kernels. The reason why these two factors must be present is because the first scales how large the neighbors' social influence is and the latter adjusts the strength of the signal from a particular location according to the distance away from the reference individual. To give a more detailed description of how each of these equations are formed, the equations from submodel M1 are carefully analyzed below as an example.

The first point of interest is that the integration is only taken over the positive spectrum. This is because the interaction kernel is assumed to be even over the entire space and the same equation can be applied to neighbors on either side (see Figure 2.2). Therefore, an individual would feel the same magnitude of impact from a neighbor on the right and another on the left if they are equidistant from the reference individual. Because the reference individual in submodel M1 only detects those moving towards it for alignment purposes, equation (2.5) only involves the neighbors on the left that are moving right,$u^+(x-s)$, and those on the right that are moving left, $u^-(x+s)$. For a right-moving reference individual, $u^-(x+s)$ would increase the probability of a turn, while $u^+(x-s)$ would decrease the probability because the reference individual would like to align with them.

Because repulsion and attraction involve all neighbors regardless of their directions, equations (2.6) and (2.7) consider $u(x \pm s)$ for both left- and right-moving neighbors. Equation (2.6) quantifies how a right-moving individual is repulsed by its neighbors. Naturally, a higher number of individuals to the right would increase the turning probability. Similarly, a higher number of individuals to the left would decrease the turning probability, since the reference individual would like to stay on the same track to avoid the others. The equations describing repulsion and attraction are identical because these two social interactions act like exact opposites of each other. When considering the attraction influences, one simply needs to take the calculations for the repulsion signals and negate the results. The same logic can be applied to find the turning probabilities of a left-moving individual under the influence of the repulsion, alignment, and attraction interactions. As well, the equations related to the other submodels can be derived using the same method as above using the interaction rules given in Figure 2.1.

This is only one of the submodels considered by Eftimie *et al.*, and there are four other submodels as shown in Figure 2.1. The following section offers an overview of the results and how they can be applied.

2.3 Discussion of the Eftimie Model

With the Eulerian model, Eftimie *et al*. have been able to establish the criteria for pattern formation analytically. Although these results will not be discussed in relation to the numerical implementation of the Lagrangian version, they are an important part of the Eftimie model. Using equations (2.1) and (2.2), the steady states of the system can be found. Furthermore, q_{al}, the strength of the alignment signal, is determined to be a bifurcation parameter determining whether one, three, or five steady states are possible. The dispersion relation can also be calculated. This is useful for the purposes of examining how the parameters affect the stability of each steady state. For example, by increasing the attraction zone, it is found that fractionation in the population decreases and larger subgroups are formed. This is a biological realistic behavior, as an increase in the attraction zone would allow animals to sense each other at larger distances. Therefore, animals would be less likely to separate from each other. Analytical results show that spatially inhomogeneous patterns can be stable steady states, and the numerical results reflect this conclusion.

The numerical investigations of the Eftimie model have produced a wide range of movement behaviors, including traveling and stationary pulses as well as traveling trains (see panels 1, 2, 5, and 6 of Figure 2.3), which have been previously produced by models without the direction dependence. The abundance of aggregation patterns occurs in spite of the model's simplicity and choice to ignore factors like the social structure within an animal group and higher dimensions. With the added consideration of direction dependence, new patterns like breathers, feathers, and zig-zag pulses ([9], [10], [11]) as shown in panels 8, 4, and 7 respectively of Figure 2.3. Feathers are pulses where individuals near the boundaries are moving in and out, and breathers are where individuals near the boundary can escape while the the rest of the group travels in a zig-zag pulse. After a while, because the boundary conditions are periodic, those that have escaped must re-join the group. Figure 2.3 illustrates the full range of results displayed by the various submodels.

By transitioning between different parameter spaces, we can examine how an animal may change its behavior according to its changes in the external environment. For example, prey animals often move in a zig-zag pattern in an attempt to be unpredictable and confusing to a predator. In fact, the group may fragment into smaller fractions so that the danger of one entire population being eaten is reduced. However, they are usually able to re-group into one single traveling pulse again after the threat of predation is removed. Animals that display such defense mechanism include the European hare, nandu, ptarmigan, jack snipes, and snipes ([15]). An alternating series of traveling and stationary pulses is another example that demonstrates animals transitioning between different behaviors. In this case, the patterns represent a group of animals migrating in one direction and taking breaks in between. Thus far, only the general framework of the Eftimie

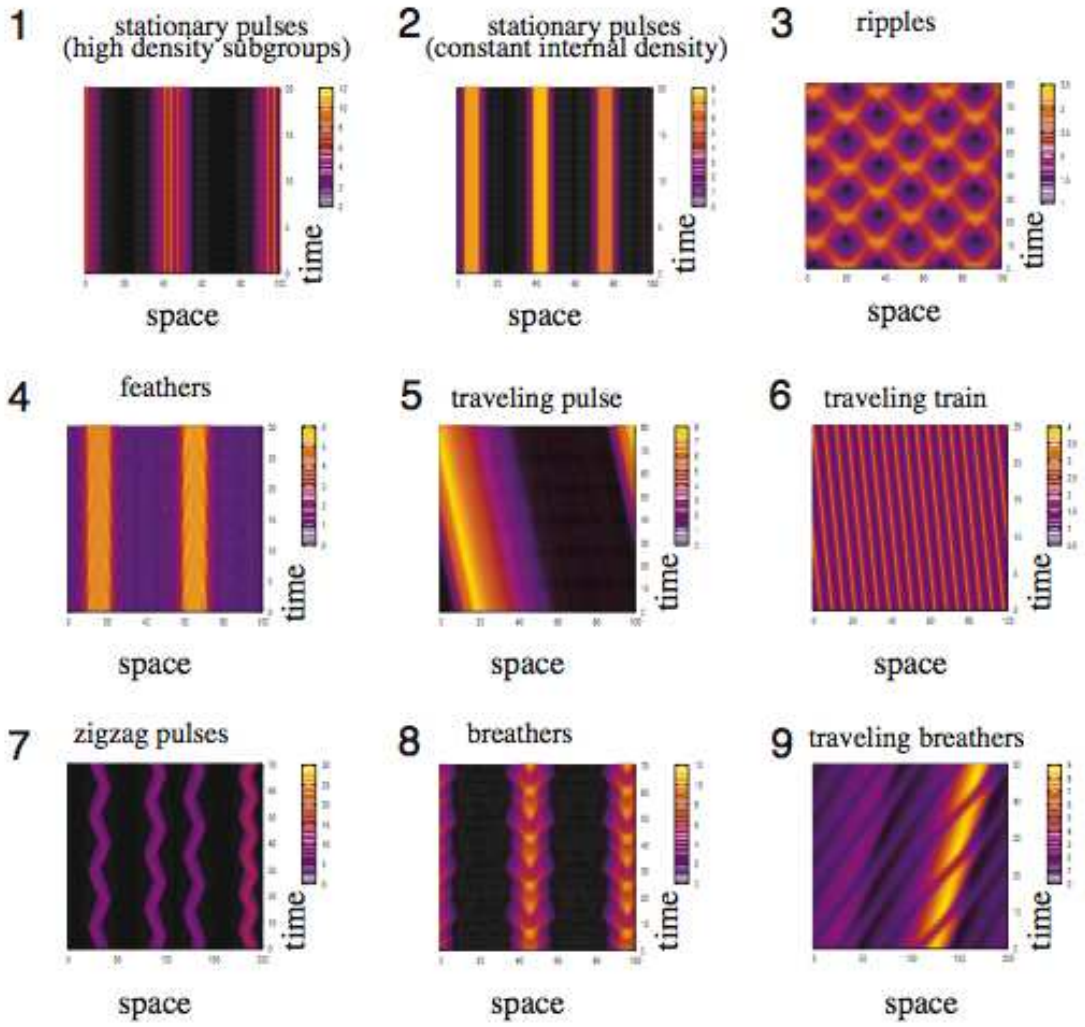

Figure 2.3: Results of the Eftimie Eulerian model. See submodels M1-M5 in Figure 2.1. The above figure is taken from [9].

PDE model can incorporate both of these behaviors by changing the parameter space.

One additional feature of the Eftimie Eulerian model is the asymmetry of interaction influence from neighbors on the left and the right. Precisely, Eftimie *et al*. incorporates two additional parameters, p_r and p_l, into the signal functions, $y^{\pm}$, to assign the strength of the interaction signals from the left and from the right. As an example, equation (2.5) is shown in this modified form with the introduction of $p_{r,l}$:

$$y_{al}^{+} = q_{al} \int_0^{\infty} K_{al}(s)(p_r u^{-}(x+s) - p_l u^{+}(x-s))ds, \tag{2.9}$$

$$p_r \neq p_l. \tag{2.10}$$

All of the other signal functions are modified in a similar fashion. The consequence of this modification is most evident in the zig-zag pattern, where the group transitions from an unbiased random movement to a biased movement.

With the wealth of behavioral patterns that the Eftimie model produces, it is logical to continue exploring the general framework of the movement model with the direction-wise communication mechanism. A question is whether or not an individual-based model can also generate the same patterns or even produce new patterns. This is the focus of the Lagrangian model, which will be discussed in the following chapter.

Chapter 3

The Lagrangian Model

3.1 Introduction

In this chapter, we explain how the Lagrangian formulation is derived from the Eftimie Eulerian model. The key question is how we can preserve the properties of the original formulation as much as possible while discretizing the system in both space and time. This problem would recur in numerous stages while building the Lagrangian model. How should the pseudocode be written to replicate the animals described by the Eftimie model? How should we translate the infinite Gaussian kernels into discrete-space functions? What is the best way to calculate the integral of the neighbor's signals as a finite sum? More importantly, after incorporating all the modifications needed for the discrete model, would the results be similar to those of the Eulerian model, except with a change in the parameter space? Each of these questions are investigated in this chapter.

In Section 3.2, we will demonstrate that the PDE Eulerian model is actually based on a group of animals moving in 1-D space with constant speed. Understanding the fundamental behavior of the individual modeled with the equations would allow us to portray the system more accurately with the pseudocode. In Section 3.3, we further explore the aspect of writing a suitable computational scheme by reviewing previous models that are similar in the set-up of the interaction zones and communication mechanisms. After setting up the numerical implementation, we must ask ourselves several questions. What boundary conditions should be used? How should we discretize space and time, and how would our choice affect the outcome of the model? We will tackle these two issues in Sections 3.4 and 3.5 respectively. In Sections 3.6, 3.7, and 3.8, we explain the interaction kernel choices and discuss the patterns generated. The first kernel is a uniform kernel, the second is a piece-wise linear function in the shape of a triangle, and the third is a normalized Gaussian function with a cut-off value. We expect that the normalized Gaussian function would produce

more similar results to the Eftimie model, given that it has a greater similarity to the original continuous Gaussian interaction kernel. After the investigation with the three kernels, we modify the Lagrangian model by incorporating asymmetry in signal reception and present our results in Section 3.9. Finally, we discuss our findings in Section 3.10.

3.2 Model Derivation

Because the PDE system from the Eftimie model is derived from a set of interaction rules that describes how an animal determines whether or not to turn, it makes the model very suitable for simulations with a discrete time and space system. With a Lagrangian formulation, the approximations that arise from generating a PDE system are avoided, and this is a general advantage of using an individual-based model.

To fully understand this system, it is important to derive the equations from first principles in the discrete time and space version. The first step is to set up a 1-D spatial system with grid-size Δx. Also, in this model, all the animals move simultaneously after a time-step of Δt. Therefore, the master equations can be given by the following, with the variables $u^{\pm}$ and $\lambda^{\pm}$ as defined previously:

$$u^+(x,t+\Delta t) = u^+(x-\Delta x,t)(1-\lambda^+\Delta t)+u^-(x+\Delta x,t)\lambda^-\Delta t, \tag{3.1}$$

$$u^-(x,t+\Delta t) = u^-(x+\Delta x,t)(1-\lambda^-\Delta t)+u^+(x-\Delta x,t)\lambda^+\Delta t, \tag{3.2}$$

where Δt is the time-step and Δx is the grid-size. Equations (3.1) and (3.2) respectively calculate the population of right- and left-moving individuals. For example, in equation (3.1), the total sum of right-moving individuals includes the adjacent left-moving neighbors to the right who decided to change direction and the adjacent right-moving neighbors to the left who kept their orientation after the previous time step. This assumption implies that the animals first move according to their designated orientation and then decide whether to turn or not at each time step. Equation (3.2) is formulated similarly.

Here, we explain the procedures taken to translate the discrete system into the continuous form given by equations (2.1) and (2.2). As an example, we will derive equation (2.1) from equation (3.1). One can perform similar steps to find equation (2.2) starting from (3.2). First-order Taylor series expansions are taken for the terms $u^+(x,t+\Delta t)$ and $u^{\pm}(x\pm\Delta x,t)$ around $u(x,t)$ in equation (3.1):

$$u^+(x,t)+\Delta t\frac{\partial u^+}{\partial t}(x,t) = (u^+(x,t)-\Delta x\frac{\partial u^+}{\partial x}(x,t))(1-\lambda^+\Delta t)+(u^-(x,t)+\Delta x\frac{\partial u^-}{\partial x}(x,t))\lambda^-\Delta t+O(\Delta x^2,\Delta t^2). \tag{3.3}$$

Because space and time increments are taken to be infinitesimally small to derive a continuous system, it is justifiable to neglect the higher order terms in the following steps. Then, we expand equation (3.3) and

divide by Δt to arrive at the following:

$$\frac{\partial u^+}{\partial t} + \frac{\Delta x}{\Delta t}\frac{\partial u^+}{\partial x} = -\lambda^+ u^+ + \lambda^+ \Delta x \frac{\partial u^+}{\partial x} + u^-\lambda^- + \lambda^- \Delta x \frac{\partial u^-}{\partial x}. \tag{3.4}$$

To transform the discrete system into the continuous system, we must take the limit where both Δx and Δt approach zero. In addition, we define the following quantity:

$$\gamma = \lim_{\Delta x, \Delta t \to 0} \frac{\Delta x}{\Delta t}. \tag{3.5}$$

Finally, after taking the limits, equation (3.4) arrives at the final form seen in equation (2.1). These calculations show that the Eftimie model is derived from the master equations (3.1) and (3.2). Note that the master equations do not involve the γ speed parameter seen in the PDE system yet. In fact, speed is implicitly present in equations (3.1) and (3.2) via the choice of Δx and Δt.

In the Lagrangian model, we try to preserve the Eftimie model as much as possible while translating it into a discrete time and space system. Since time is discrete, the turning probability is determined at each time step for every individual according to the same functions, $f^{\pm}(y^{\pm}(r, al, a))$ and $\lambda^{\pm}(y^{\pm})$, used in the Eulerian version. The basic computational scheme is similar to that of Kolpas *et al.* ([18]) and Couzin *et al.* ([4]), in which the individuals' locations are stored in a vector and updated every time step according to their directions. We introduce the pseudocode and calculations used to discretize the Eulerian model and transform it into a Lagrangian model in Section 3.3.

3.3 Numerical Implementation

In this section, we give a detailed account of how the discrete formulation of the Eftimie model is modified from the Kolpas model, previously discussed in Section 1.2.4. The numerical implementation of the Kolpas model can be easily adapted for use with the Eftimie model. The reason is that both models share the same underlying assumptions. Namely, they model animals in 1-D space with turning rates that are influenced by the interaction signals from their neighbors in three zones, the repulsion, alignment, and attraction zones. However, we must also recognize that the Eftimie model is more complicated in its calculation of the turning probability with additional considerations like the direction-wise communication mechanisms. Therefore, we will discuss the key components in the Kolpas scheme that requires modification for application in the Eftimie model.

The Kolpas formulation assumes that alignment and attraction is considered only if repulsion is absent. In contrast, the Eftimie model considers all three social interactions simultaneously. In fact, it assigns

three variables, q_a, q_{al}, and q_r, to describe the strengths of the social interactions, attraction, alignment, and repulsion, respectively. The Eftimie model also assumes that certain neighbors are weighted more in the interactions, as seen by the Gaussian interaction kernel in the continuous formulation. The repulsion, alignment, and attraction zones in the Eftimie model can overlap, while the Kolpas model does not allow for this feature. In this section, we will explain how we calculate the turning probabilities for the Eftimie model. Except for the calculation of the turning probabilities, the numerical implementation of the Eftimie model will follow that of the Kolpas model.

Since the Lagrangian formulation of the Eftimie model tracks the movement of an animal individually, we will explain the numerical implementation from the same point of view. Each animal is described by two quantities, its position x_i and velocity v_i, where the index i indicates the individual being referred to. According to the model derivation described in Section 3.2, the animals first update their positions and then decide whether or not to turn. They move according to the following equation:

$$x_i = x_i + sv_i, \tag{3.6}$$

where s adjusts how far forward the individual moves every time step. Then, the individuals continue with the process of examining their surroundings to determine the desired orientation.

The interactions between neighbors and individuals are similar to that in the Eulerian version, but the width of the interaction zones can now be defined by the number of grid-points, as seen in Figure 3.3. The set up of the interaction zones identical to the continuous-space version, where the repulsion zone is located closest to the individual and the attraction zone is the farthest. Each social interaction, repulsion, alignment, and attraction, contribute to the turning probability. Each animal scans through all the interaction zones for any neighbors and decide whether or not to change direction accordingly. We use a right-moving individual in submodel M1 to explain the steps in the numerical simulation.

First, the repulsion signal is calculated via the following equation:

$$y_r^i = \sum_{x_j \in Z_{r_i}} K_r(|x_j - x_i|), \tag{3.7}$$

where Z_{r_i} denotes the repulsion zone of the i^{th} individual, and K_r is the interaction kernel for repulsion, which will be further explained in Sections 3.7 and 3.8. The attraction signal is calculated in a similar fashion:

$$y_a^i = \sum_{x_j \in Z_{a_i}} K_a(|x_j - x_i|), \tag{3.8}$$

where Z_a denotes the attraction zone of the i^{th} individual. The calculation of both the attraction and repulsion signals is very similar to that of the Kolpas model, except for the incorporation of the interaction

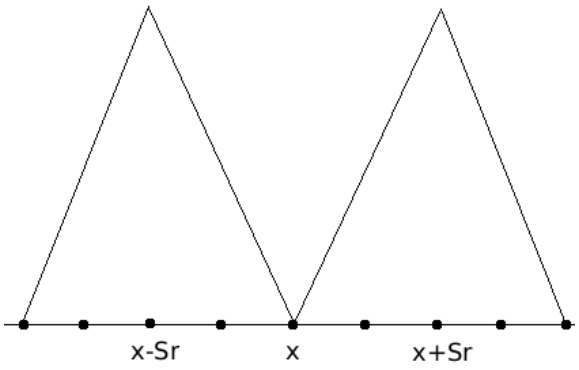

Figure 3.1: How animals measure their interaction zones in the Lagrangian formulation. Animals now measure distance in terms of number of grid-points.

kernels to consider spatial effects on signal strengths. This is because the rules of submodel M1 dictate that all neighbors in the attraction and alignment zones are to be considered.

The calculation of the alignment signal will be different due to two reasons. First, for the purposes of alignment, we consider the neighbors' velocities instead of their locations. Second, we will only consider neighbors who are moving towards the reference individual. In other words, the right moving individual considers two distinct groups for alignment: the right-moving neighbors in the left alignment zone, Z_{left,al_i}, and the left-moving neighbors in the right alignment zone, Z_{right,al_i}.

$$y_{al}^{i} = \sum_{v_j<0, x_j \in Z_{right,al_i}} K_{al}(|x_j - x_i|) - \sum_{v_j>0, x_j \in Z_{left,al_i}} K_{al}(|x_j - x_i|), \tag{3.9}$$

When all the interaction signals are known, we use equations (2.4) and (2.3) to evaluate the turning probability, namely $\lambda^{i,+}(y_{r,al,a}^{i})$. The individual-based approach allows us to use a uniform random variable, X, to determine whether or not the animal turns. Specifically,

$$v_i(t+\tau) = \begin{cases} v_i(t), & X > \lambda^{i,+}, \\ -v_i(t), & \text{otherwise.} \end{cases} \tag{3.10}$$

With the uniformly generated random variable X, we incorporate stochastic effects, which is one of the advantages of the Lagrangian formulation. Like the original Eftimie model, $y_{r,al,a}$ are varied depending on the submodel and its communication mechanisms. The process of updating position and direction is repeated for each individual until a pattern is established.

One of the issues regarding the numerical implementation yet to be discussed is the choice of boundary conditions, which will be explored in the following section.

3.4 Boundary Conditions

Like the Eftimie Eulerian model, the Lagrangian model uses periodic boundary conditions. An interpretation of the periodic boundary condition is that the animals are on a circular domain. In this case, the model may be describing animals living on a mountain at a particular altitude, insects that travel around a plant or tree stalk, or aquatic animals traveling around an island. From another point of view, using periodic boundary conditions allows us to simulate a system infinitely large in area. This is an effective method for reducing the computational time when modeling very large populations.

The reason is that, by using periodic boundary conditions, we are essentially repeating the data on the domain and connecting them consecutively so that an animal at one end of the domain would feel the influence of an animal at another end. The implications of this assumption is that the habitat being examined does not contain any spatial inhomogeneities or edge effects that may affect the animal movement. Only the data on the function domain $[0, L]$ is available, but for the simulations to run with the periodic boundary conditions, we need to consider the influences of neighbors outside the domain for the animals living close to the boundaries, $x = 0, L$. To extend the domain when incorporating these external influences into the signal functions $y^{\pm}(u^{\pm})$, we set $u(x + L, t) = u(x, t)$.

In addition, we must consider where to stop considering the neighbors outside the function domain. In other words, with the assumption that $u(x + nL, t) = u(x, t)$, where $n = 0, 1, ..., \infty$, the calculation of the signal functions from the neighbors would be extremely computational expensive. This is due to the fact that the Gaussian kernel with no compact support in the Eulerian model implies that every neighbor, no matter how far away, contributes to the turning probability. Therefore, we must choose some reasonable limit where the interaction kernel becomes negligible to reduce the computational cost of using periodic boundary conditions. To reproduce the results in the Eftimie model, only the periodic boundary conditions are used because they were the only ones explored extensively in the original work.

3.5 Space and Time Discretization

An interesting aspect that has arisen from the discretization of the original Eftimie model is the missing parameter γ. According to equation (3.5), γ is the ratio of the spatial step to the grid-size in the limit where both values approach zero. In other words, γ can be regarded as a measure of the speed all the animals are traveling at. With the Lagrangian formulation, because we are no longer using an infinitesimally small grid-size and time step to make the system variables continuous, there is no explicit parameter for speed that plays a role in the numerical simulations. However, the Lagrangian formulation has two additional numerical

parameters that are of concern: Δt and Δx, which are the time and spatial increments respectively.

The first numerical parameter, Δt, does not change the patterns generated. That is because Δt is not explicitly involved in the numerical simulation in Section 3.3. Further, it is implicitly implemented because each iteration, involving the decision to change direction and update in position, represents one time step. If Δt does not play a role, then how do we adjust the speed of the individuals? To answer this question, we look at equation (3.6).

To vary the speed, we need to adjust step size and not the time increment, as previously discussed. However, the definition of the Lagrangian formulation does not require for discrete space; it simply implies that the model tracks the animals' movement from an individual point of view. In fact, there is no limitation on what speed the animal travels at. We are thus motivated to use s in equation (3.6) to designate the distance that an animal travels per time step, which is effectively, the speed.

Interestingly, we find that an optimal speed must be used for the animals to be able to aggregate. When the speed is too fast, the animals have a tendency to move away from each other very quickly, and no consistent pattern can be found. When the speed is too slow, the same patterns form, but a longer time period is needed to observe the formation of these patterns. Therefore, to optimize the results range and computational time, the default speed is set to be 0.1, which corresponds to the speeds used by Eftimie *et al*. To emphasize the need to use an appropriate speed, we vary the parameter s while keeping all other model parameters constant. The impact of speed on the patterns generated is clear in Figure 3.2, which displays three different results depending on the value of s. In the case where the speed is too slow, the algorithm must run for twice as long compared to the optimal speed to achieve the same equilibrium zig-zag state (see Figure 3.2a,c). In the case where the speed is too high, it is difficult to observe any aggregation between the individuals (see Figure 3.2b).

The default value of γ is set at 0.1 because this is in the range of values used for γ in the original PDE model. We also do not put an emphasis on the speed because the focus of this project is to investigate how different communication mechanisms lead to different aggregation behaviors. Therefore, only the three parameters related to the strength of these interactions, $q_{r,al,a}$, are varied in the simulations, whereas the other parameters are simply kept at constant values that allow for pattern formation.

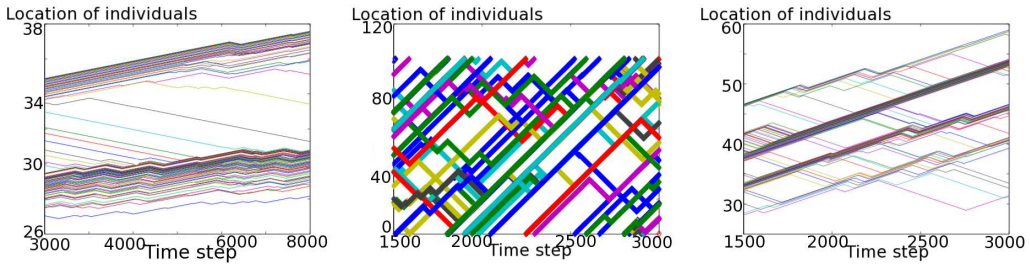

(a) (b) (c)

Figure 3.2: The effect of speed on the aggregation patterns. (a) Low speed (s=0.01); (b) high speed (s=1); (c) optimal speed (s=0.1). Each trace represents an individual's trajectory. For small s (a), we observe a zig-zag pulse after a long transient period. For large s (c), aggregation behavior is lost. When the speed is at an intermediate value (b), the individuals form zig-zag pulses after a short transient period.

3.6 The Uniform Kernel

As a starting point for exploring the Lagrangian model, the simplest option is a uniform kernel. The uniform kernel is given by:

$$\hat{K}_i(s) = \begin{cases} \frac{1}{2m_i}, & s \in [s_i - m_i, s_i + m_i], \\ 0, & \text{otherwise.} \end{cases} \tag{3.11}$$

s_i is the centre of each interaction zone, and m_i defines the width (see Figure 3.3). The uniform kernel does not vary the impact of neighbors at different locations within the interaction zones. Only traveling and stationary pulses are found as shown in Figure 3.4.

3.7 The Triangular Kernel

Motivated by the results of the previous section, a triangle is a suitable candidate for the shape of the interaction kernel. The equation for this interaction kernel as a piecewise linear function of space is given by the equation below (see Figure 3.5.)

$$\hat{K}_i(s) = \begin{cases} 1 - |\frac{s - s_i}{m_i}|, & s \in [s_i - m_i, s_i + m_i], \\ 0, & \text{otherwise.} \end{cases} \tag{3.12}$$

Thus far, only the zig-zag, traveling, and stationary pulses have been observed from the Lagrangian implementation of all the submodels. Not a single submodel can produce all four patterns. Submodels M1, M2, and M4 are the ones with the greatest pattern range, generating three aggregation patterns. The details

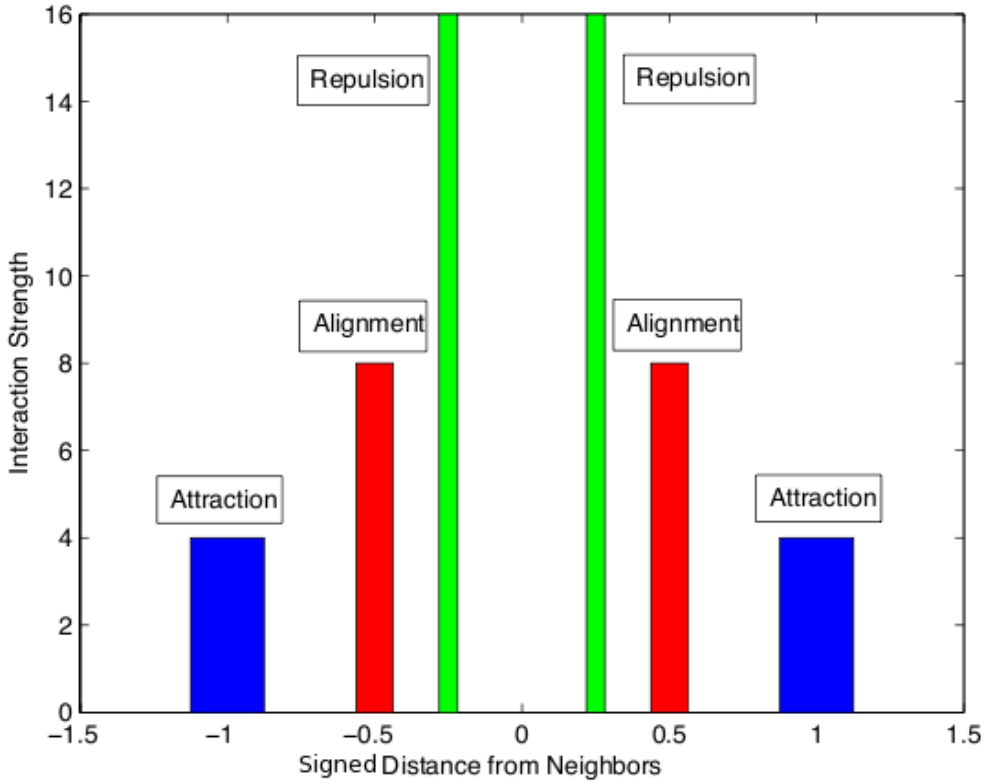

Figure 3.3: The uniform kernel. Each curve is a uniform kernel used in the Lagrangian model described by equation (3.11). $s_r = 0.25, s_{al} = 0.5, s_a = 1, m_{r,al,a} = \frac{s_{r,al,a}}{8}$.

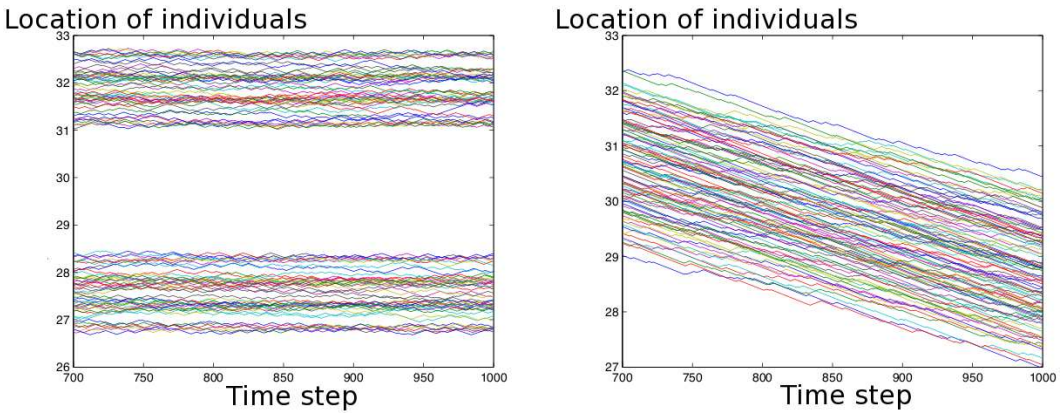

(a) (b)

Figure 3.4: Patterns produced by the uniform kernel using submodel M1. (a) Stationary pulses wtih $q_{al} = 0$. (b) Traveling pulse with $q_{al} = 1$. All other parameters are $\lambda_1 = 0.2, \lambda_2 = 0.9, q_r = 1, q_a = 1, s_r = 0.25, s_{al} = 0.5, s_a = 1$, and $m_{r,al,a} = \frac{s_{r,al,a}}{8}$.

and implications of the results will be further discussed, but first, we must have a clear description of each of these patterns.

To better compare the results between the Eulerian and Lagrangian models, we explain the definitions of different behavioral patterns. We will only be discussing those that exist for both formulations, which are the stationary, traveling, and zig-zag pulses so far. When there is one group that travels in one consistent direction, it is a traveling pulse. In the definition of the stationary pulses, it is irrelevant how many groups the animals have aggregated in. As long as the individuals remain in the same general area, we define them as stationary pulses.

The zig-zag pattern is a pattern that has not been observed by other mathematical models. The zig-zag pulse is simply where the main group, like the stationary pulse, remains in the same general vicinity. However, this is now caused by the entire group changing its direction periodically (see grid 7 in Figure 2.3). The semi-zig-zag pattern is not included in Figure 2.3, but it is one of the results found by the Eftimie model ([9], [10], [11]). Here, the animals transition in and out of being stationary pulses and traveling pulses. Specifically, they repeat the cycle of traveling in one direction consistently before remaining still for a short period of time. This seems to mimic immigration in a grand scale with breaks incorporated.

With the behavioral patterns formally defined, we discuss the results produced by two different interaction kernels in the following sections. The first is a triangular interaction kernel, and the second is a cut-off Gaussian kernel. Also, we offer some explanations why only some patterns are produced.

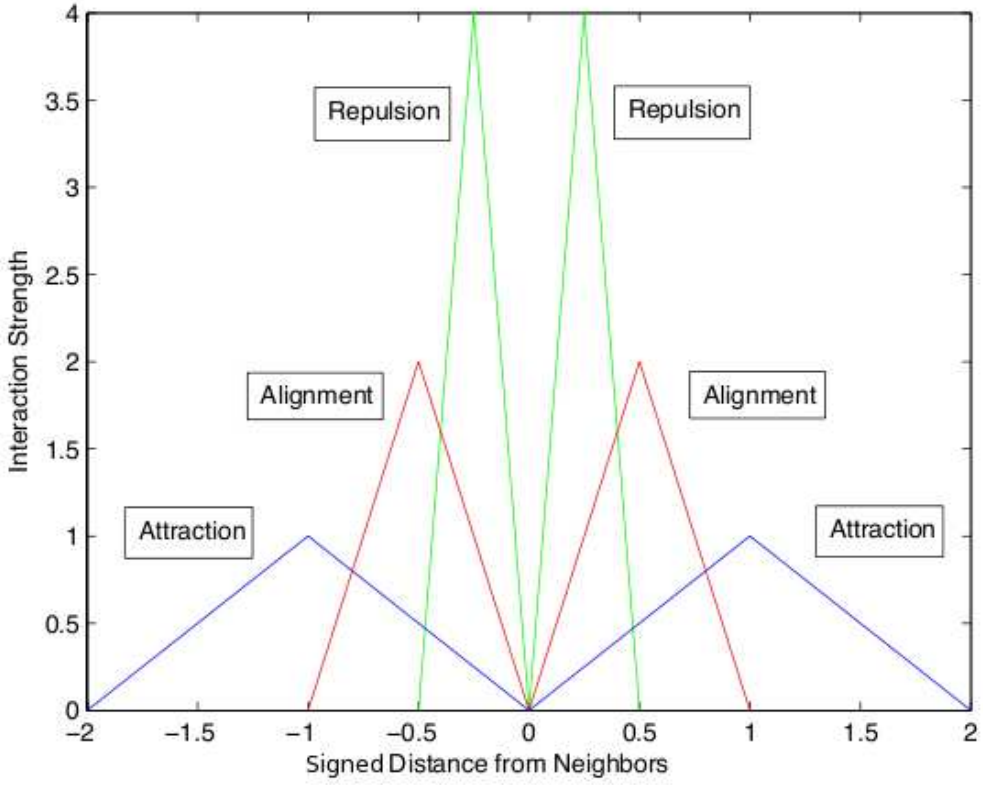

Figure 3.5: Triangular interaction kernels. These curves are the kernels used in the Lagrangian model described by equation (3.12). Parameters: $s_a = 1, s_{al} = 0.5, s_r = 0.25, m_j = \frac{s_j}{8}$ in the Gaussian kernel and $m_j = s_j$ in the discrete formulation, $j = r, al, a$.

Submodel	Stationary pulse (large groups)	Stationary pulse (small groups)	Traveling pulse	Zig-zag pulse
M1	Y	Y	Y	N
M2	Y	Y	Y	N
M3	Y	N	Y	N
M4	Y	Y	N	Y
M5	N	N	Y	N

Table 3.1: Results produced with the triangular kernel.

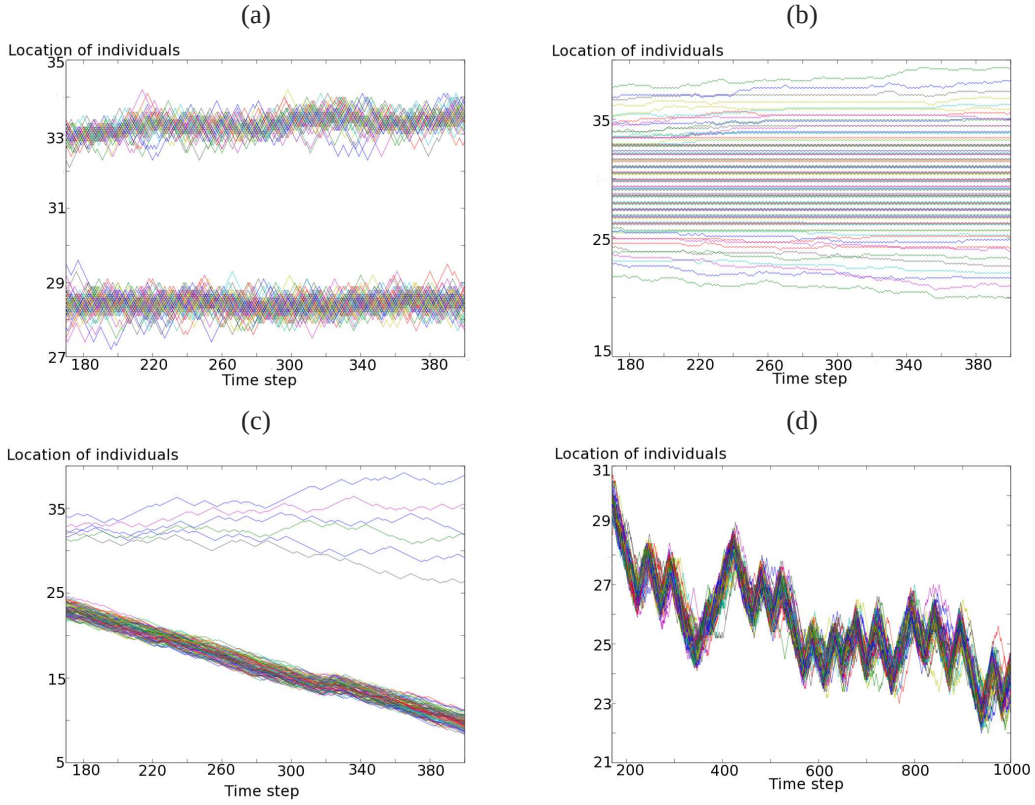

Figure 3.6: Patterns obtained with the Lagrangian model with triangular kernels. (a) Stationary pulse (large groups); (b) stationary pulse (small groups); (c) traveling pulse; (d) zig-zag pulse. In (a) and (c), animals form stationary pulses. In (b), we observe a traveling pulse with a small population of strayers. In (d), the animals travel in a zig-zag pulse. Parameters used in (a). M1: $\lambda_1 = 0.4, \lambda_2 = 1.8, q_r = 0.5, q_{al} = 0.9, q_a = 0.7$. (b) M2: $\lambda_1 = 1.33, \lambda_2 = 6, q_r = 0, q_{al} = 1, q_a = 1$. (c) M3: $\lambda_1 = 1.33, \lambda_2 = 6, q_r = 10, q_{al} = 0.1, q_a = 10$. (d) M4: $\lambda_1 = 0.2, \lambda_2 = 0.9, q_r = 20, q_{al} = 0, q_a = 19$. In all of the above cases, $s_r = 0.25, s_{al} = 0.5, s_a = 1$, and $m_{r,al,a} = s_{r,al,a}$.

Figure 3.6 shows four different behaviors found with the triangular kernels, and every trace shows an individual trajectory. In panel (a), large stationary pulses are shown. Here, the animals are not stationary, although the group as a whole remains in the same neighborhood. In fact, the individuals vary their locations within the group, and sometimes they may even deviate from the main group. However, the animal is always able to return to the main group because of its neighbors' attraction signals. In panel (b), small stationary pulses are shown. Here, the animals are in small groups of only two or three. The groups are in close proximity to each other, but there is no merging behavior.

In panel (c), a traveling pulse is shown. Interestingly, there is a group that has strayed away and remained uninfluenced by the main group. A few individuals have deviated enough from the population so that it is outside the attraction zone of the members in the traveling group. The emergence of this separate subgroup is a rare phenomenon in this model because usually wandering animals cannot escape the sink formed by the attraction zones of the group, which forces escapees to head towards the centre of the crowd. Therefore, the initial departure is a result of the inherent stochasticity in how the animals choose to turn using a uniformly distributed random number. A question to ask is whether the strayers would be able to re-join the main group due the periodic boundary conditions. To answer this, we run the simulation for a longer period of time so that the main group arrives at the left domain boundary, re-enters at the right domain boundary, and continues traveling in a pulse towards the strayers. In submodel M3, the animals can only receive communication signals from the neighbors in front of them. Therefore, the strayers should be able to sense the main group after it has passed in front of them. Whether or not they decide to change their direction to re-join the larger group depends on the relative sizes of the strayers and the main group. It is observed that the main group must be sufficiently large to form an attraction force strong enough to pull the strayers back in.

In panel (d), the animals aggregate in a zig-zag pattern. This is another behavior where the stochasticity in the Lagrangian model is highlighted. In the zig-zag patterns found by the Eulerian formulations, animals change directions periodically, and the group moves back and forth about the same center. In panel (d), the individuals do not turn in a predictable manner, and the general direction that the zig-zag travels in appears to be random.

A general trend is that a larger λ_1 and λ_2 reduces the size of aggregations. This is because individuals change direction at a higher frequency and this makes traveling consistently in one direction unlikely, discouraging merging behavior. There must also be a balance between λ_1 and λ_2, for an increase in λ_1 means that the animal is more likely to turn, even without any signals from neighbors. Therefore, if $\lambda_2 > \lambda_1$, the effects of the communication mechanism can be overwhelmed by this constant turning probability.

Some of the behaviors can be formed with only two social interactions. For example, submodel M4 can produce zigzag pulses and stationary pulses without alignment. This echoes the results of some of the previous Lagrangian models discussed where not all of the three social interactions are used ([6], [20], [21], [30]). Submodel M3 shows some interesting behavior where individuals are more easily lost because only those who are heading towards the reference individual are considered in the social interactions.

Submodel M5 produces the smallest range of behaviors (it can only generate zig-zag pulses) because it considers the smallest number of neighbors, specifically only those are who are ahead and moving towards

Submodel	Traveling pulse	Stationary pulse	Biased zig-zag pulse	Unbiased zig-zag pulse	Breather
M1	Y	Y	N	N	N
M2	Y	Y	N	N	N
M3	Y	Y	N	N	Y
M4	Y	Y	Y	Y	N
M5	N	N	Y	N	N

Table 3.2: Results produced with the Gaussian cut-off kernel.

the reference individual. With this restriction, it is not surprising that other submodels can produce more patterns. The original Eftimie model and the Lagrangian implementation both share the result that submodel M5 only produces one aggregation behavior.

3.8 The Cut-off Gaussian Kernel

Another option for the interaction kernel is to simply choose a cut-off value for which the Gaussian interaction kernels are assumed to be zero. This would give an interaction kernel with a shape that is closer to that used in the Eftimie model. The essential difference is that in the continuous model, because the Gaussian kernel does not have compact support, the individuals are assumed to have no limit in their ability to detect neighbors far away. In the discrete version, with the introduction of the cut-off value, the individuals can only sense neighbors in a defined neighborhood. Since the discrete version aims to reproduce the results of the Eulerian formulation, the cut-off value is chosen to be half of the total domain size. This implies that the individual can see all of its neighbors because it is assumed to look in both directions to determine the turning probability. Through this action, the individual scans the entire domain without counting the same neighbor twice with the periodic boundary conditions. The following equation, therefore, is another sensible choice for an interaction kernel that is to be tested:

$$\hat{K}_i(s) = \begin{cases} \frac{1}{2\pi m_i^2} \exp(\frac{-(s-s_i)^2}{2m_i^2}), & s \in [s_i - \frac{dom}{2}, s_i + \frac{dom}{2}], \\ 0, & \text{otherwise}, \end{cases} \tag{3.13}$$

where dom is the total domain size.

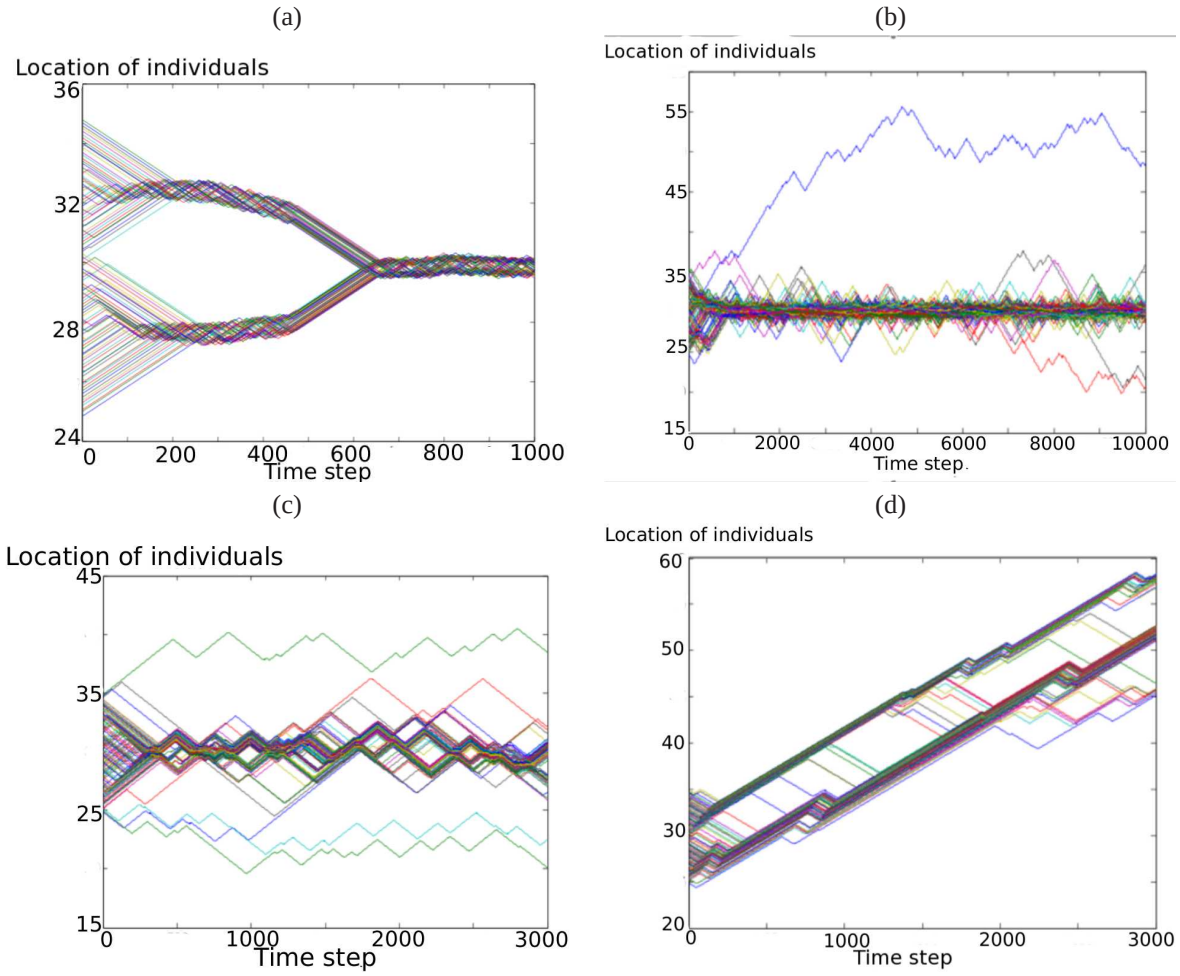

Figure 3.7: Results of Lagrangian model with cut-off Gaussian kernel. (a) Stationary pulse; (b) breather; (c) unbiased zig-zag pulse; (d) biased zig-zag pulses. In (a), we observe a stationary pulse. Panel (b) shows a breather, where animals temporarily deviate from the main group before being drawn in by the attraction force. In (c), there is an unbiased zig-zag pulse, where the animals remain in the same general vicinity. This is different from the biased zig-zag pulse in (d), where the group's position is shifting to the right. Parameters used in (a). M3: $\lambda_1 = 0.2, \lambda_2 = 0.9, q_r = 4, q_{al} = 30, q_a = 30$. (b) $\lambda_1 = 0, \lambda_2 = 0.8, q_r = 30, q_{al} = 0, q_a = 10$. (c) M5: $\lambda_1 = 0, \lambda_2 = 0.8, q_r = 50, q_{al} = 30, q_a = 50$. (d) M4: $\lambda_1 = 0, \lambda_2 = 0.8, q_r = 50, q_{al} = 30, q_a = 50$.

Results are shown in Figure 3.7. In panel (a), the stationary pulse shows non-constant interior density. There are more animals at the boundary compared to the center. Also, we see how two groups merge because their attraction zones overlap, causing the two pulses to gravitate towards, and eventually, join each other.

In panel (b), breathers, which have not been found with the triangular kernels, are shown. Here, animals can actually deviate quite far away from the main group before returning. This is the main difference separating it from the stationary pulse, where animals can only travel a small distance away before being pulled back to the main group by attraction. In panel (c), we see the zig-zag pulse again, with no directional bias. In panel (d), the biased zig-zag pulse shows animals traveling in one direction between short, temporary switches to traveling in the opposite direction.

Comparing the parameters used for the Gaussian kernel and the Lagrangian kernel, we see that the Gaussian kernel formulation requires that λ_2 is zero for aggregation to occur. Using a non-zero λ_2 with the parameter sets eliminates any patterns. This indicates that with the Gaussian kernel, we must emphasize the effects of the communication mechanism by ignoring any constant turning probability. Even when λ_1 is zero, panels (b) and (c) show that stochastic effects alone can cause loss of individuals from the main group.

With this kernel, there is a larger range of movement pattern observed, similar to that of the Eftimie model. In general, submodels M1 and M2 produce the usual patterns seen in most movement models, like traveling and stationary pulses. Submodels M3, M4, and M5 generate some of the new pattens from the Eulerian model, like breathers, and zig-zag pulses.

3.9 Asymmetry in Communication Mechanisms

One of the aspects that the Eftimie model explored is asymmetry in communication mechanisms, as mentioned in Section 2.3. Essentially, the individuals sense neighbors on one side stronger than on the other, which is described in equation (2.9). The following equation expresses the same scenario in discrete space:

$$y_{al} = p_r \sum_{v_j<0, x_j \in Z_{right,al_i}} K_{al}(|x_j - x_i|) - p_l \sum_{v_j>0, x_j \in Z_{left,al_i}} K_{al}(|x_j - x_i|), \tag{3.14}$$

$$p_r \neq p_l. \tag{3.15}$$

Like the Eulerian formulation, the repulsion and attraction signals are modified in a similar fashion to incorporate asymmetry.

However, in patterns like the traveling and stationary pulses, the asymmetry does not produce a noticeable change. To observe the effects of varying the influence from neighbors on the right and the left, we use the zig-zag pulse. Figures 3.8(b) and 3.8(c) show the group behavior when the signal strength is stronger on one side than the other. As a result, the zig-zag pulse is biased towards the side where the interaction signals are stronger. When the interaction signals are the same strength on either side, the group forms a zig-zag pulse that moves about in the same area (Figure 3.8(a)).

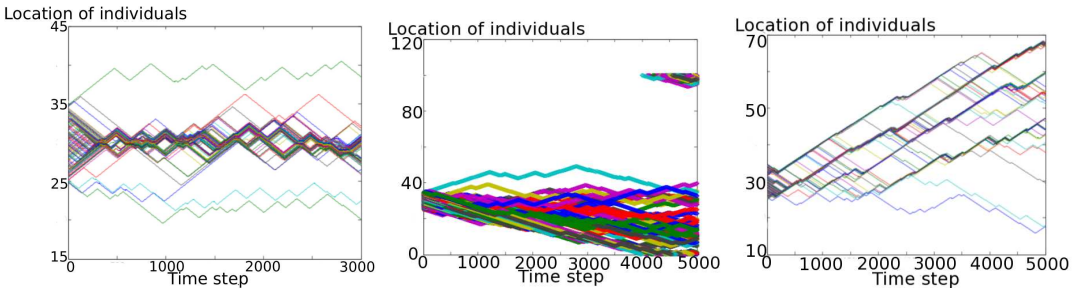

(a) (b) (c)

Figure 3.8: The effect of asymmetry on the zig-zag pattern. (a) $p_l = p_r$; (b) $p_l > p_r$; (c) $p_l < p_r$. If $p_l = p_r$ (a), the animals sense neighbors on each side equally and therefore form a symmetric pattern where the main group has no biased tendency to move left or right. Therefore, the zig-zag pulse remains in the same general vicinity. If $p_l > p_r$ (b), the animals travel to the left. If $p_l < p_r$ (c), the animals travel to the right.

3.10 Discussion

In this chapter, we investigated how we transform the original continuous-time and space movement model into a discrete-time and space formulation using the same master equations that govern the turning probabilities based on interactions with neighbors. The Lagrangian model has succeeded in generating some of the patterns found in the Eulerian model, with the zig-zag and breather pulses never before produced by any other individual-based model. In addition to these new patterns, we have also found the traveling and stationary pulses. Feathers, ripples, and and traveling trains are not found.

The reason that not all patterns from the Eulerian model are generated may be simply due to the effects of the discretization or the changes made to the interaction kernels. On the other hand, this may also be because the parameter space was not explored sufficiently. This is where the advantages of the Eulerian formulation become evident. With the application of bifurcation theory, Eftimie *et al*. are able to determine the relevant parameter ranges for the existence of various steady states. In a Lagrangian model, we can only run multiple simulations with various parameter sets to find different aggregation patterns.

Comparing Figures 3.7 and 3.8 to Figure 2.3, we see that stochastic effects play a much more significant role in the Lagrangian formulation. This is demonstrated by the fact that none of the patterns from the original model displays any random loss of individuals from the main group. Also, an interesting feature in Figure 2.3 is that we can observe the gradients in the population, where the group can smoothly transition between a dense to a sparse area. With the Lagrangian formulation, we do not observe this phenomenon.

The simulations with the triangular and Gaussian interaction kernels have generated encouraging results, which bring us to the following question. If the system now describes animals moving in continuous time using the same movement and communication principles, what patterns would we observe? Would the parameters have the same impact as in the Lagrangian formulation? What is the most accurate way to translate Eftimie's PDE model into an ODE model? With these questions in mind, we investigate pattern formation in a discrete-space, continuous time system in the following chapter.

Chapter 4

Pattern Formation in a Discrete-Space, Continuous-Time System

4.1 Introduction

In [9], [10], and [11], the individuals were modeled interacting and traveling in a continuous-time, continuous space system. In the previous chapter, the same set of interaction rules were taken to produce a Lagrangian system with discrete-time and discrete-space. The further question to investigate is how the behavior compares if the individuals were described by a continuous-time and discrete-space system. The derivation of this model would require taking the PDE system developed in [9], [10], and [11] and translating the equations into a set of ODEs for each spatial point considered. In the following sections, we will describe how the ODE set is formed and the results of the simulations.

In Section 4.2, we derive an ODE system from the PDE system in the Eftimie model. Then, in Section 4.3, we present the aggregation patterns generated by this ODE model.

4.2 Numerical Implementation

Similar to the original Eftimie model, we have two populations to track: the left-moving and right-moving individuals. Therefore, the solution is described by two vectors with lengths determined by the grid-size; one vector, $\vec{u}^+$, contains the number of right-moving individuals at each grid-point, while the other one, $\vec{u}^-$, records the number of left-moving individuals at each grid-point.

The system that is to be discretized over space is given by equations (2.1) and (2.2), and the model is to be considered over a finite 1-D domain divided into a total of n grid-points with periodic boundary conditions.

Time then becomes the only continuous variable, allowing the application of a Matlab ODE solver. This technique is referred to as the method of lines. To express the spatial derivatives with finite differences, the upwind-downwind schemes must be considered so that the discretization is consistent. Since equation (2.1) and (2.2) describe right and left-moving individuals respectively, it is clear that the backward difference must be used for equation (2.1) and the forward difference must be used with equation (2.2). The reason is clear when we consider the available information on a particular individual's previous traveling history. For example, given one entry in $\vec{u}^+$, it is known that these individuals in the relevant grid-point would be in the left adjacent grid-point at the previous time-step. As a consequence, only the backward discretization scheme can be used because no information is given for the number of individuals in the right adjacent grid-point at the previous time-step. The discretization can be described by the following equation:

$$\frac{\partial u^+}{\partial x} = \frac{u_i^+ - u_{i-1}^+}{\Delta x} + O(\Delta x), \tag{4.1}$$

$$i = 1, ..., n, \tag{4.2}$$

where the index i indicates the grid-point along the domain being described. (Note that this definition is different from that used in Chapter 3, where i refers to the individual.) Similarly, one entry in $\vec{u}^-$ would only contain information about the number of individuals in the right adjacent grid-point at the previous time-step. Here, the forward discretization scheme must be used:

$$\frac{\partial u^-}{\partial x} = \frac{u_{i+1}^- - u_i^-}{\Delta x} + O(\Delta x), \tag{4.3}$$

$$i = 1, ..., n. \tag{4.4}$$

The discretization scheme used has a first-order approximation error. Using a higher-order scheme like the central difference approximation is not possible because such schemes require past information from both sides of the relevant grid-point, which is not possible when the directionality of an animal determines that information is only given on one side.

Using equations (4.2) and (4.4), equations (2.1) and (2.2) can be transformed into the following system of ODEs:

$$\frac{du_i^+}{dt} + \gamma\frac{u_i^+ - u_{i-1}^+}{\Delta x} = -\lambda^+ u_i^+ + \lambda^- u_i^-, \tag{4.5}$$

$$\frac{du_i^-}{dt} - \gamma\frac{u_{i+1}^- - u_i^-}{\Delta x} = \lambda^+ u_i^+ - \lambda^- u_i^-. \tag{4.6}$$

After rearranging the terms, the following ODE system is found:

$$\frac{du_i^+(x)}{dt} = -\gamma(\frac{u_i^- - u_{i-1}^-}{\Delta x}) - \lambda_i^+ u_i^+(x,t) + \lambda_i^- u_i^-(x,t), \tag{4.7}$$

$$\frac{du_i^-(x)}{dt} = \gamma(\frac{u_{i+1} - u_i}{\Delta x}) + \lambda_i^+ u_i^+(x,t) - \lambda_i^- u_i^-(x,t), \tag{4.8}$$

$$i = 1, ..., n. \tag{4.9}$$

The turning probabilities, $\lambda^{\pm}$, must be calculated for each spatial point and traveling direction. To calculate this turning probability, we use the same equations given in the Eftimie model (see equations (2.3) and (2.4)). The numerical integration method used to approximate the integral of the interaction kernels is the composite Simpson's rule, restricting n to be an even number. To achieve this, we define a vector $\vec{K}$ representing the kernel strength, whose entires are given by:

$$\hat{K}_i(x_j) = \begin{cases} 4K_i(x_j), & \text{if } j \text{ even and } j \in (1, \frac{n}{2}), \\ 2K_i(x_j), & \text{if } j \text{ odd and } j \in (1, \frac{n}{2}), \\ K_i(x_j), & \text{if } j = 1, \frac{n}{2}, \end{cases} \tag{4.10}$$

where $i = r, al, a$ and $j = 1, ..., \frac{n}{2}$. Here x_j are the grid-points along the function domain. Assuming that the total domain size is L, x_j can be defined as $\frac{Lj}{n}$. $\vec{K}$ only goes through half of the total domain because an individual only scans through half the domain when looking to the left or to the right. Depending on the particular submodel, the neighbors who determine the turning probability vary. To illustrate exactly how the turning probability is calculated for a reference individual, an example is given.

Assuming that the individual follows the interaction rules given by submodel M1, there are two different interaction modes. Essentially, attraction and repulsion follow the same interaction mode, where all neighbors are considered regardless of their orientations, while alignment is in a different category; only the neighbors who are moving towards the reference individual are considered. To be clear which neighbors are relevant, four vectors are defined: $\vec{u}^{\pm}_{right}$ and $\vec{u}^{\pm}_{left}$. The subscripts, left and right, indicate where the neighbor is located with respect to the reference individual. In other words, $\vec{u}^{\pm}_{right}$ would be simply the vector formed by taking all the entries that follow the reference location in the vectors $\vec{u}_{\pm}$. For example, if the reference location is x_j, then $\vec{u}^{\pm}_{right}$ would be $\vec{u}^{\pm}$ from the index $j+1$ to n, and $\vec{u}^{\pm}_{left}$ would be $\vec{u}^{\pm}$ from the index 1 to $j-1$. Since the boundary conditions are periodic, to ensure that $\vec{u}^{\pm}_{right}$ and $\vec{u}^{\pm}_{left}$ have the same number of entries, we can shift a section of the longer vector to the shorter one (see Figure 4.1). For instance, if $\vec{v}^{\pm}_{right}$ are longer than $\vec{u}^{\pm}_{left}$, then we would shift right-most entry in $\vec{u}^{\pm}_{right}$ to $\vec{u}^{\pm}_{right}$ as the right-most entry until the vectors are of the same length. Similarly, if $\vec{u}^{\pm}_{right}$ are shorter than $\vec{u}^{\pm}_{left}$, then we would shift left-most entry in $\vec{u}^{\pm}_{left}$ to $\vec{u}^{\pm}_{left}$ as the left-most entry. We can perform these operations because the model is applied with periodic boundary conditions.

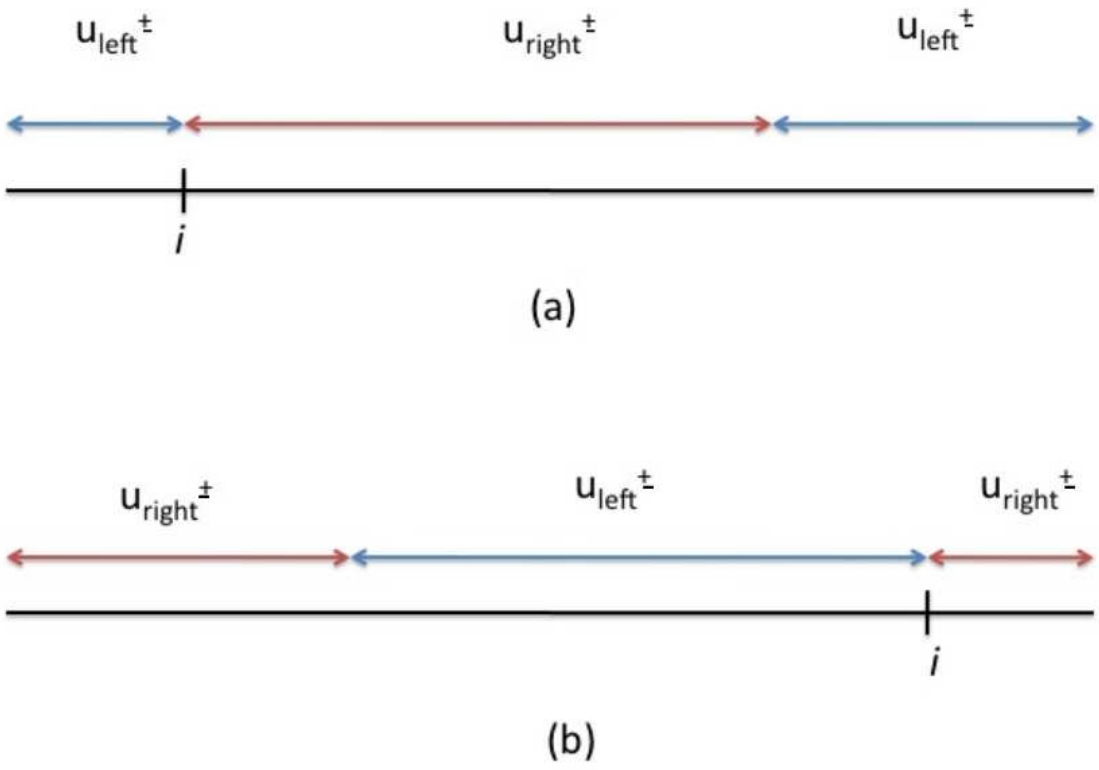

Figure 4.1: In case (a), the individual is situated in the left side. Therefore, $\vec{u}^{\pm}_{left}$ wraps around the left end and extends into the right end of the domain to have the same length as $\vec{u}^{\pm}_{right}$. Similarly, case (b) shows that $\vec{u}^{\pm}_{right}$ wraps around the right end and extends into the left end of the domain when the reference individual is situated in the right side.

Here, we take submodel M1 as an example for calculation of $y^+_{r,al,a}$, and the reference location is x_j.

$$y^+_{i,al} = q_{al}(\vec{K}_{al}\dot{(}\vec{u}^-_{right} - \vec{u}^+_{left})), \tag{4.11}$$

$$y^+_{i,r,a} = q_{r,a}(\vec{K}_{r,a}\dot{(}\vec{u}_{right} - \vec{u}_{left})). \tag{4.12}$$

The signals for the various submodels can be formulated similarly. The turning probability is then calculated using the same functions as the Eftimie model with equations (2.3) and (2.4).

After having calculated the turning probabilities, the ODE system can simply be solved numerically by Matlab using the function ode45, which is based on an explicit Runge-Kutta (4,5) formula and the Dormand-Prince method. The Runge-Kutta (4,5) formula, used for solving ODE with initial conditions given, is an explicit adaptive-size formula that minimizes the error by calculating and then comparing the results found with a Runge-Kutta-4 and Runge-Kutta-5 method, both requiring six function evaluations at each time step. As a result of using the Dormand-Prince method, a fifth-order solution is produced. It is important to recognize the numerical errors in our methods used for solving the ODEs because this helps us realize where the differences in patterns formed with the PDE and ODE models arise.

4.3 Results using Discrete Space, Continuous Time Formulation

Since the ODE formulation is an intermediate version, we anticipate that the results would include patterns that have been found in both of the Lagrangian and PDE models. Specifically, the traveling, stationary, and zig-zag pulses are expected. However, with the ODE simulations, an unexpected result previously unseen in the Eulerian PDE formulation is that a homogeneous solution is generated with most parameter sets used in the PDE simulations for inhomogeneous patterns like breathers and traveling pulses. This may be a consequence of the additional numerical errors incorporated due to the space discretization. In fact, if λ_1 is large, meaning that there is a significant random component incorporated into the turning probability, it is difficult to find an inhomogeneous distribution. This implies that with a space discretization, random effects may be already incorporated into the system and an increase in the random turning probability overwhelms the effects of the turning signals from neighbors.

When the random turning probability, λ_1, is reduced, more spatial patterns are formed. The patterns found include traveling and stationary pulses, traveling trains, breathers, and traveling breathers. Traveling breathers have not been produced by the previous discrete-space-and-time formulations. These patterns are shown in Figure 4.2, and the color scale is a representation of the population density. For example, in panel (a) with stationary pulses, all the colored lines remain at the same location for each time step, which means that the animals have aggregated in stationary groups.

Submodel	Traveling pulse	Stationary pulse	Traveling train	Breather	Traveling breather
M1	Y	Y	Y	N	N
M2	Y	Y	N	N	N
M3	Y	N	N	N	Y
M4	Y	N	N	N	Y
M5	Y	Y	N	Y	Y

Table 4.1: Results produced by ODE formulation.

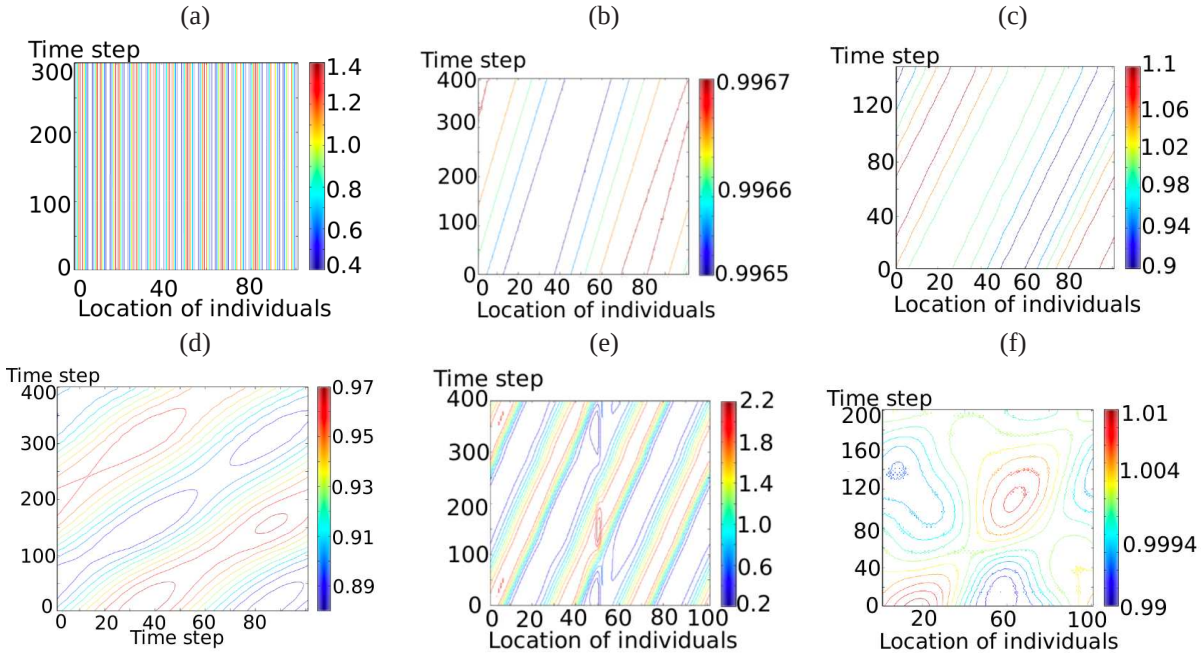

Figure 4.2: Results of Lagrangian ODE model. (a) Stationary pulse; (b) traveling pulse; (c) traveling train; (d) traveling breathers; (e) traveling breather; (f) breathers. $\Delta = \gamma = 0.1$ in all figures. Other parameters used in (a) M1: $\lambda_1 = 0.2, \lambda_2 = 0.9, q_r = 10, q_{al} = 5, q_a = 10$. (b) M2: $\lambda_1 = 0.4; \lambda_2 = 1.8, q_r = 0.2, q_{al} = 2, q_a = 2$. (c) M3: $\lambda_1 = 0, \lambda_2 = 6, q_r = 5, q_{al} = 2, q_a = 5$. (d) M3: $\lambda_1 = 0, \lambda_2 = .9, q_r = 2, q_{al} = 2, q_a = 6$. (e) M5: $\lambda_1 = 0, \lambda_2 = .9, q_r = 10, q_{al} = 5, q_a = 10$. (f) M5: $\lambda_1 = 0, \lambda_2 = .9, q_r = 0, q_{al} = 30, q_a = 30$.

Interestingly, zig-zag pulses could not be found at all, while traveling breathers are a prevalent pattern for submodels M3-5 in spite of its absence in the previous Lagrangian formulations. In panels (a) and (b) of Figure 4.2, the population density is displayed, where the animals are in a stationary and traveling pulse. In the traveling trains in panel (c), the animals are separated into two different groups while moving in the same direction. This pattern was very rare because in most cases, traveling groups joined into one traveling pulse. There are two ways that animals move in traveling breathers, one from submodels M3-4 and another from submodel 5. In panel (d), the traveling breathers consist of animals who periodically move towards and away from the center of the group. In panel (e), the groups of animals mostly travel in a straight line, but some at the edge periodically move outwards before re-joining their group to form a single file again. Not all of the groups exhibit this behavior, and those who do may not display the same degree of expansion and contraction. For example, the groups in the centre of the domain exhibit more fluctuations in the size than those closer to the boundary of the domain.

Having explored the discrete-space-and-time, ODE, and PDE formulations, we can now take a look at incorporating direction-dependent communication in other Lagrangian models that have a different approach to modeling animal movement. In the following chapter, we use the Kolpas model as the modeling framework while adding components from the Eftimie model. Would the model produce the same patterns as the Eftimie model or the Kolpas model? What trends would this hybrid model share with its predecessors? These are key questions that we explore.

Chapter 5

A Eftimie-Kolpas Hybrid Model: Prioritizing Repulsion

5.1 Introduction

The Kolpas model, as previously discussed in subsection 1.2.4, shares many features as the Eftimie model. Both consider repulsion, alignment, and attraction between individuals, but the Kolpas model does not have a direction-dependent component in the interactions. Another significant difference in the assumptions for the Kolpas model is that individuals prioritize repulsion over alignment and attraction. Individuals in the Kolpas model consider alignment and attraction only if there are no neighbors in the repulsion zone, as illustrated in Figure 5.1. We assume that animals move at a constant speed of ± 1. Kolpas found that the size of the alignment zone determines whether the group is stationary or traveling. When the size of the alignment zone is small, animals are in the stationary phase. As the size of the alignment zone increases, the animals are more likely to be traveling. The Kolpas model shows that for an intermediate size in the alignment zone, animals spontaneously switch from the stationary and traveling phases (see Figure 5.2). Kolpas termed this behavior stick-slip.

To understand animal aggregation behavior, we incorporate direction-dependent communication mechanisms from the Eftimie model into the modeling framework of Kolpas *et al.* and investigate whether or not animals can spontaneously transition between different behaviors using only one parameter set, similar to the stick-slip behavior in the Kolpas model. A question that is answered at the same time is whether or not more patterns can be produced from the Kolpas framework if the direction-dependent mechanism is incorporated.

In Section 5.2, we combine the Kolpas and Eftimie models. In particular, we discuss the modifications

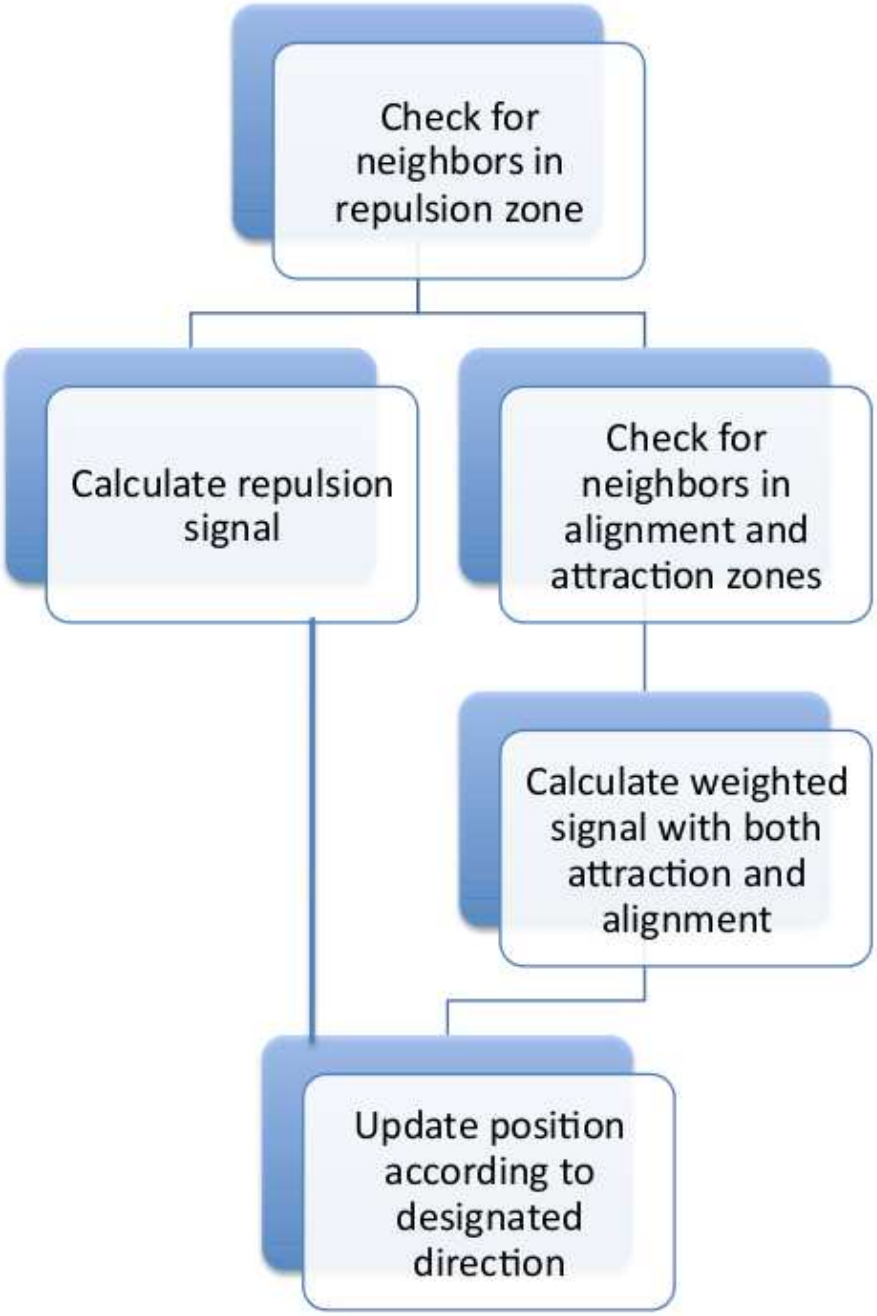

Figure 5.1: The decision-making process of the Eftimie-Kolpas hybrid model. The individuals scan the alignment and attraction zones only if the repulsion zone is empty.

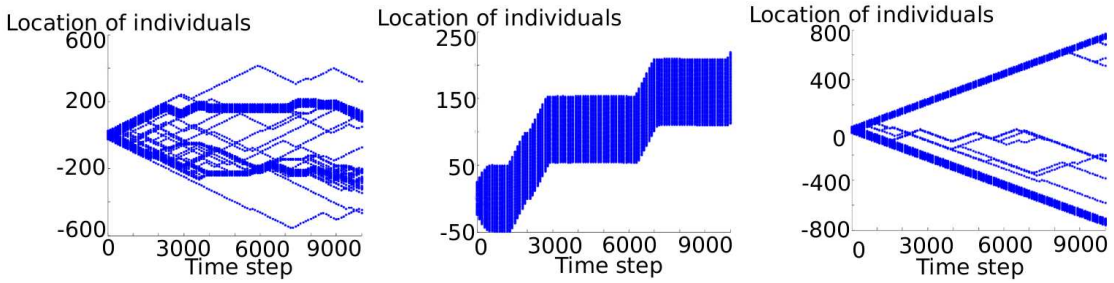

(a) (b) (c)

Figure 5.2: The behaviors of the Kolpas model. (a) Small alignment zone with size of 0.1 unit; (b) intermediate alignment zone with size of 0.6 unit; (c) large alignment zone with size of 1.1 unit. Each blue line represents an animal's trajectory. The animals travel when the alignment zone is large (c) and remain stationary when the alignment zone is small (a). For an alignment zone of intermediate size, they spontaneously switch between the two phases (b). This behavior is called stick-slip.

introduced into the Kolpas framework and explain why these changes are significant. Then, we present results from two different implementations in Section 5.3. Finally, we discuss the implications of our results in Section 5.4.

5.2 Building the Eftimie-Kolpas Hybrid

An important consideration in building the Eftimie-Kolpas hybrid is to determine what assumptions from the Eftimie model should be incorporated into the Kolpas model. Since the distinguishing feature of the Eftimie model is the direction-dependent communication mechanism, we choose to incorporate it in our hybrid model. Therefore, the first step is to find what behaviors the Kolpas model can generate if we apply the communication mechanisms described by Figure 2.1. Here, we use the Kolpas modeling scheme from subsection 1.2.4 as our starting point.

Equations (1.8) and (1.9) must be modified depending on the submodel implemented. These are equations from the Kolpas model that calculate the interaction signals, the former considering repulsion and the latter attraction and alignment. Equation (1.9) is applicable only if the repulsion zone is completely empty. To demonstrate how they must be changed to include a direction-dependent component, we show the equations for communication signals of submodel M1. Because animals take into account all neighbors in the repulsion zone, equation (1.8) remains the same. However, to send alignment signals, the neighbor must be moving towards the reference individual in the relevant interaction zone. According to this requirement,

equation (1.9) is modified into:

$$V = \frac{v_i(t) + \sum_{c_j(t) \in Z_{al_j}(t), v_i(t)(c_j(t)-c_i(t))<0} v_j(t)}{|v_i(t) + \sum_{c_j(t) \in Z_{al_j}(t), v_i(t)(c_j(t)-c_i(t))<0} v_j(t)|} + \sum_{c_j(t) \in Z_{a_j}(t)} \frac{c_j(t) - c_i(t)}{|c_j(t) - c_i(t)|}. \tag{5.1}$$

The additional condition in the alignment term, $v_i(t)(c_j(t) - c_i(t)) < 0$, means that neighbors in the alignment zone must be moving towards the reference individual in order to be detected.

For notational convenience, we define the notation $*_i$, where $i = r, al, a$, to represent the conditions that the neighbors must satisfy to be considered in the social interactions. With this notation, equation (5.1) can be rewritten as:

$$V = \frac{v_i(t) + \sum_{*_{al}} v_j(t)}{|v_i(t) + \sum_{*_{al}} v_j(t)|} + \sum_{*_a} \frac{c_j(t) - c_i(t)}{|c_j(t) - c_i(t)|}, \tag{5.2}$$

where $*_{al} = c_j(t) \in Z_{al_j}(t), v_i(t)(c_j(t) - c_i(t)) < 0$ and $*_a = c_j(t) \in Z_{a_j}(t)$. The conditions vary according to the submodel, but they all share the common feature that the neighbor must be within the relevant interaction zone.

Another question is whether or not we should further develop our hybrid by adding interaction kernels and parameters to assign the weights of the interactions. The results from the Lagrangian implementation of the Eftimie model imply that interaction kernels play an important role in finding a larger pattern range. To determine whether this also applies to the Eftimie-Kolpas hybrid, we simulate animal motion with and without interaction kernels. In the Eftimie model, the group exhibits various grouping behaviors according to the different weights assigned to each interaction. In contrast, the Kolpas framework always prioritizes repulsion over alignment and attraction, meaning that we can only adjust the significance of alignment and attraction but not repulsion. We introduce the parameter $\tilde{q}_a$, which is the relative strength of attraction compared to alignment.

In summary, if the repulsion zone is not empty, we use the following equation to determine the individual's velocity:

$$V = -\sum_{*_r} K_r(|c_j(t) - c_i(t)|) \frac{c_j(t) - c_i(t)}{|c_j(t) - c_i(t)|}. \tag{5.3}$$

Otherwise, the individual proceeds to scan the alignment and attraction zones to calculate its direction:

$$V = \frac{v_i(t) + \sum_{*_{al}} K_{al}(|c_j(t) - c_i(t)|) v_j(t)}{|v_i(t) + \sum_{*_{al}} K_{al}(|c_j(t) - c_i(t)|) v_j(t)|} + \tilde{q}_a \sum_{*_a} K_a(|c_j(t) - c_i(t)|) \frac{c_j(t) - c_i(t)}{|c_j(t) - c_i(t)|}. \tag{5.4}$$

The definitions of $K_{r,al,a}$ remain unchanged from equation (3.13), and the final velocity is calculated according to equation (1.10), which normalizes the velocity to a value of ± 1. Periodic boundary conditions are used in all of the simulations to ensure that the animals remain within a confined region, increasing the

probability that they are close enough to interact with each other. In contrast, the Kolpas model does not use any boundary conditions because it simulates animal movement on an infinite domain. Its results do not show many strayers, therefore eliminating the possibility of losing group members.

5.3 Aggregation Patterns of the Eftimie-Kolpas Hybrid

In this section, we discuss two different implementations of the Eftimie-Kolpas hybrid. Their difference lies in that the one involves interaction kernels while the other does not. In Sections 5.3.1 and 5.3.2, we present the patterns generated. In all of the simulations below, we keep speed constant at 0.075 space increment per time step for easier comparison. Then, in Section 5.4, we discuss the common trends between the two implementations.

5.3.1 The Eftimie-Kolpas Model with No Interaction Kernels

In this subsection, we explore what types of behavior the Kolpas model generates if only direction-dependent communication is included. We investigate all the submodels shown in Figure 2.1. The trends discussed in this subsection can be generalized to all submodels even though we may only display results from a subset of the submodels. Like the Kolpas model, we observe three patterns for the different submodels: traveling, semi-zig-zag, and stationary pulses. It is important to recognize that the stick-slip behavior mentioned in the Kolpas model is analogous to the semi-zig-zag pulses from the Eftimie model. Both are used to describe the movement that spontaneously switches between traveling and resting. The pattern generated depends on the parameters used.

In particular, we look at the effect of varying the attraction force by adjusting the parameter $\tilde{q}_a$. As shown in Figure 5.3, we find that the attraction force acts as a glue and maintains the integrity of the group. In the case of small $\tilde{q}_a$, we observe a traveling pulse with more strayers. As $\tilde{q}_a$ is increased, strayers are pulled back into the group, and the traveling pulse gives way to semi-zig-zag solutions.

In the original Kolpas model, the behavior is controlled by the size of the alignment zone, m_{al}. According to the results from Kolpas *et al.*, we would expect that a larger alignment zone increases the tendency of the group to be in the mobile phase. To verify if this holds for the hybrid model, we vary the alignment zone for behavior generated with a large and small $\tilde{q}_a$. Results are shown in Figure 5.4. We observe that in contrast to the Kolpas model, the size of the alignment zone does not affect the general qualitative behavior of the group. For a large $\tilde{q}_a$, the group remains stationary, as shown in Figures 5.4(a)-(c). Instead, we see fewer stationary pulses spaced farther apart as m_{al} is increased. The distance between each pulse is determined by

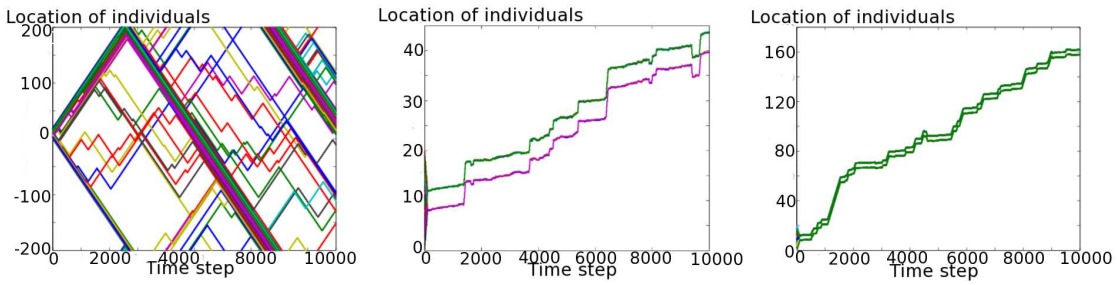

(a) (b) (c)

Figure 5.3: Different behaviors of the Eftimie-Kolpas hybrid with no interaction kernels for varying values of the relative attraction strength. (a) $\tilde{q}_a = 0.3$; (b) $\tilde{q}_a$=3; (c) $\tilde{q}_a = 30$. For a small q_a (a), a traveling pulse is formed. For an intermediate value of q_a (b), semi-zig-zag pulses are formed. For a large q_a (c), the group also forms semi-zig-zag pulses, but these are spaced further apart compared to those formed in (b). The figure shows how the aggregation behavior changes for submodel M1 as $\tilde{q}_a$ is increased. Panels (a)-(c) show different spatial scales because only the region that is explored by the animals is presented. Parameters used: $n = 100, p = 0.001, m_r = 3, m_{al} = 1, m_a = 3$.

where the attraction zone starts, as Figures 5.4(a)-(c) all display a spacing of approximately $m_r + m_{al}$. For a small $\tilde{q}_a$, as shown in Figures 5.4(d)-(f), traveling pulses are always formed. For this behavior, it is more difficult to define the edges of the pulses because there are many strayers. However, Figures 5.4(d)-(f) show that as m_{al} increases, the traveling pulse becomes less dense and more dispersed. When m_{al} is sufficiently large, the animals in the traveling pulse no longer appear to be moving in a single cohesive group. Rather, there are two files traveling in the same direction adjacent to each other, similar to the behavior shown in traveling trains (see Figure 5.4(f)).

Given that the parameter $\tilde{q}_a$ has such a profound effect on the behavior of the animals, one would expect that the size of the attraction zone also plays an important role in determining the aggregation behavior. However, this does not seem to be the case as no qualitative changes are observed as the parameter m_a is increased.

Finally, we investigate how the population would react to a larger repulsion zone. Figure 5.5 shows that as the repulsion zone becomes larger, the traveling pulses becomes less compact and there are more strayers. If m_r is sufficiently large, we predict that no aggregation would occur at all. Yet, it is most likely that this threshold value of m_r is so large that it is no longer biologically relevant. To illustrate why setting $m_r > 8$ is not realistic, we consider the scenario illustrated in Figure 5.5(c). Using a repulsion zone of eight units, animals can still form a coherent traveling pulse, despite the high number of strayers. This suggests that we should further increase m_r to test whether or not the aggregation behavior is lost after passing a certain

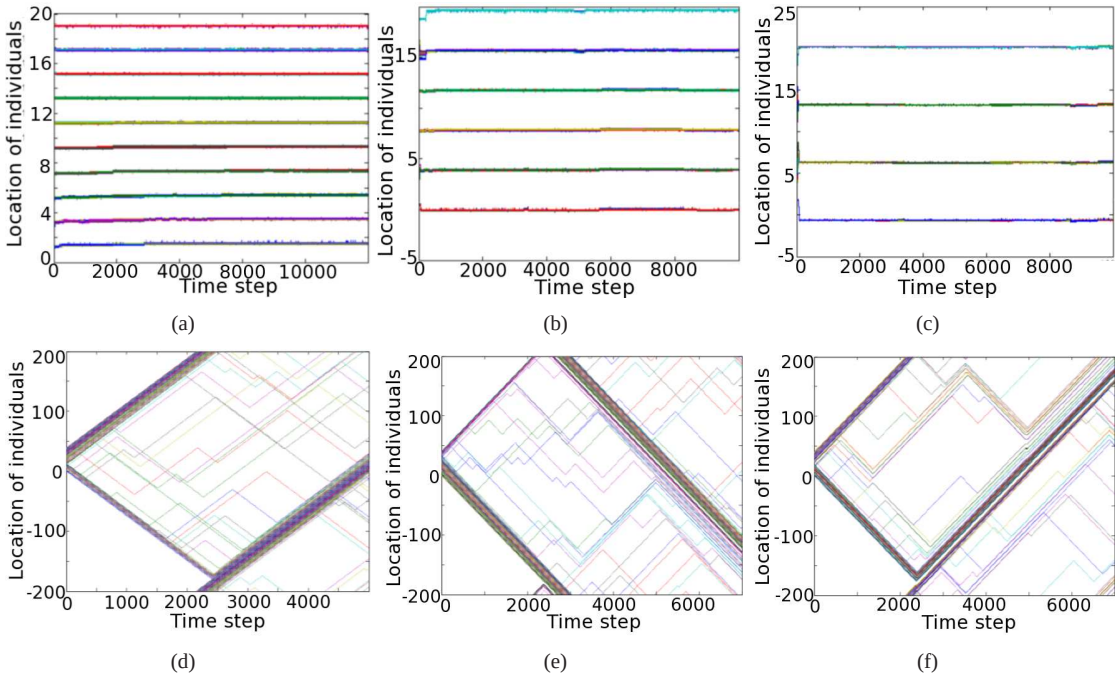

Figure 5.4: Different behaviors of the Eftimie-Kolpas hybrid with no interaction kernels for varying sizes of alignment zone. (a) $m_{al} = 1$; (b) $m_{al} = 3$; (c) $m_{al} = 6$; (d) $m_{al} = 1$; (e) $m_{al} = 5$; (f) $m_{al} = 7$. The figure shows how the aggregation behavior changes for submodel M1 as m_{al} is varied. In panels (a)-(c), stationary pulses are formed. In panels (d)-(f), traveling pulses are formed. In general, as m_{al} increases, the spacing between the pulses increases as well. Parameters used: $n = 100, p = 0.001, m_r = 1, m_a = 3$ for two values of $\tilde{q}_a$ ($\tilde{q}_a$=3 in (a)-(c); $\tilde{q}_a$=0.3 in (d)-(f)).

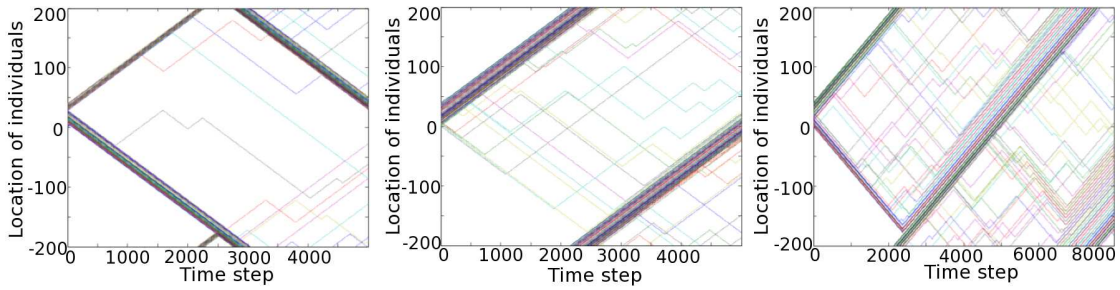

Figure 5.5: Different behaviors of the Eftimie-Kolpas hybrid with no interaction kernels for varying sizes of the repulsion zone. (a) $m_r = 0.1$; (b) $m_r = 2$; (c) $m_r = 8$. The figure shows how the aggregation behavior changes for submodel M3 as m_r is varied. For all three values of m_r used in this figure, a traveling pulse is formed. As m_r is increased, the pulse becomes less dense. Parameters used: $n = 100, p = 0.001, m_{al} = 1, m_a = 1, \tilde{q}_a = 0.3$.

threshold value. However, given that the animals move at a constant speed of 0.075 space increment at each time step, an animal would have to walk approximately 107 steps to cover a repulsion zone of eight grid-points. Therefore, it is doubtful that an animal would be repelled by a neighbor that is so far away.

Another interesting aspect to explore is whether or not all three interactions are needed for aggregation behavior. In particular, are both alignment and attraction required to keep the group together? From Figure 5.6, we can deduce that repulsion pulls the group apart, while alignment and attraction help maintain the integrity of the group. Interestingly, even though repulsion is prioritized, as long as either alignment or attraction is present, the animals can form one cohesive group. Figure 5.6(a) shows a pulse in random movement, emphasizing the importance of alignment in the formation of a traveling pulse. Figure 5.6(b) shows the traveling pulse loses individuals consistently, highlighting how attraction can act as a glue between individuals.

5.3.2 The Eftimie-Kolpas Hybrid with Cut-off Gaussian Kernels

In this subsection, we discuss the aggregation patterns generated if both interaction kernels and direction-dependent communication mechanisms are included in the Kolpas model. The first noticeable difference between the hybrid version with and without interaction kernels is the significant increase in the number of strayers when cut-off Gaussian kernels are added. This feature is especially evident in submodels M3 and M5, where aggregation behavior is lost. Animals in submodel M5 scatter especially quickly, likely due to the fact that the social interactions involve fewer neighbors when compared to submodel M3. According to

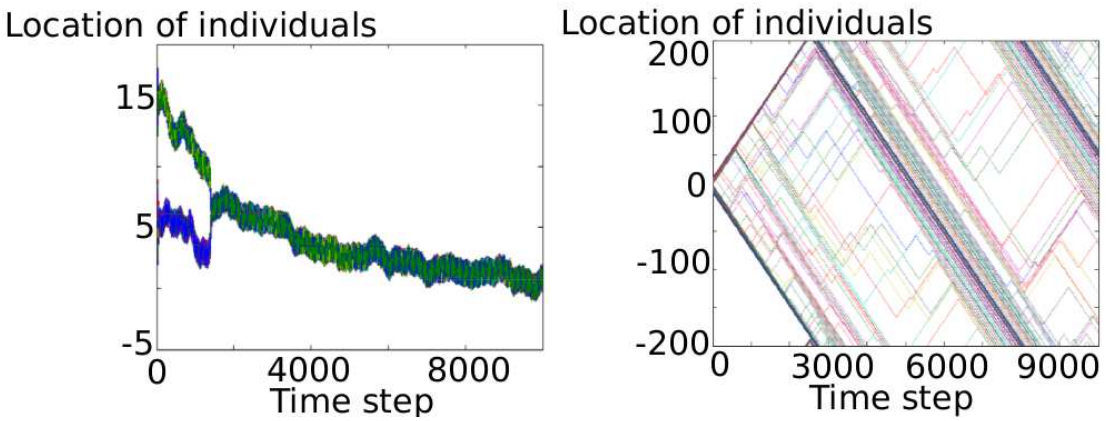

(a) (b)

Figure 5.6: Aggregation patterns for the Eftimie-Kolpas hybrid with no interaction kernels using two social interactions only. (a) $m_{al} = 0$; (b) $m_a = 0$. This figure shows that aggregation occurs as long as attraction or alignment is present. For no alignment (a), even though aggregation occurs, the individuals cannot form a traveling pulse. For no attraction (b), traveling pulses are formed. Parameters used for both figures: $\tilde{q}_a = 3, n = 100, p = 0.001$. Interaction zone sizes in Figure 5.6(a): $m_r = 2, m_a = 2$. Interaction zone sizes in Figure 5.6(b): $m_r = 2, m_{al} = 3$.

Figure 2.1, submodels M3 and M5 are the two submodels that only take into account neighbors which are in front of the reference individual. This implies that for the Eftimie-Kolpas model with cut-off Gaussian kernels, it is important to receive communication signals from both directions. Therefore, in the discussion below, we focus on submodels M1 and M4.

The first parameter that we explore for submodel M1 is $\tilde{q}_a$ (see Figure 5.7). The value of $\tilde{q}_a$ affects how cohesive the group is. When $\tilde{q}_a$ is sufficiently small, the animals cannot form groups (see Figure 5.7(a)). For larger values of $\tilde{q}_a$, the animals aggregate in stationary pulses (see Figure 5.7(b) and 5.7(c)). This is expected because attraction is the force keeping the individuals together.

For submodel M1, regarding the size of the attraction zone, we notice a different trend from the Eftimie-Kolpas hybrid without any interaction kernels. When there is no attraction force present, the group travels uniformly (Figure 5.8(a)). When there is a small attraction zone, the group exhibits stick-slip or semi-zig-zag behavior (Figure 5.8(b)). Finally, when the attraction zone is sufficiently large, the animals form stationary pulses (Figure 5.8(c)). The impact of the attraction zone on the patterns formed is reminiscent of the trend with regards to the size of the alignment zone in the Kolpas model, where animals travel for a large alignment zone and remain stationary for a small alignment zone.

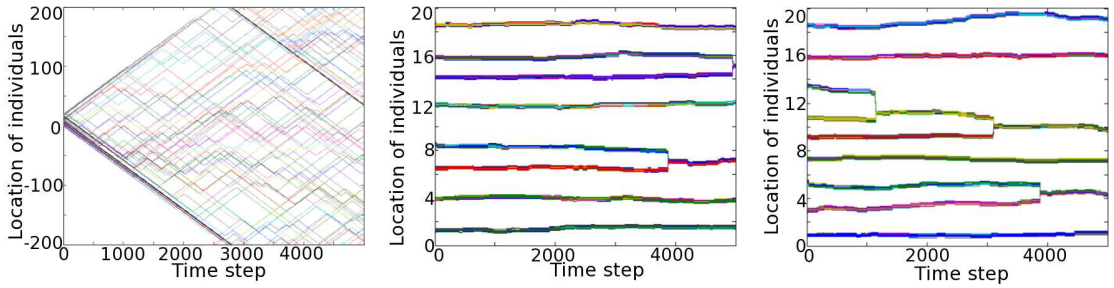

(a) Weak relative attraction signal strength. $\tilde{q}_a = 1$.

(b) Intermediate attraction signal strength. $\tilde{q}_a = 7$.

(c) Strong relative attraction signal strength. $\tilde{q}_a = 10$.

Figure 5.7: Aggregation patterns for varying values of $\tilde{q}_a$ in the Eftimie-Kolpas hybrid submodel M1 with interaction kernels. (a) $\tilde{q}_a = 1$; (b) $\tilde{q}_a = 7$; (c) $\tilde{q}_a = 10$. When $\tilde{q}_a$ is sufficiently small, aggregation behavior is lost (a). In (b) and (c), where intermediate and strong relative attraction signal strengths are applied respectively, stationary pulses are formed. The number of pulses increases as $\tilde{q}_a$ decreases. Parameters used for all three figures: $n = 100, p = 0.001, m_r = 0.1, m_{al} = 1, m_a = 1$.

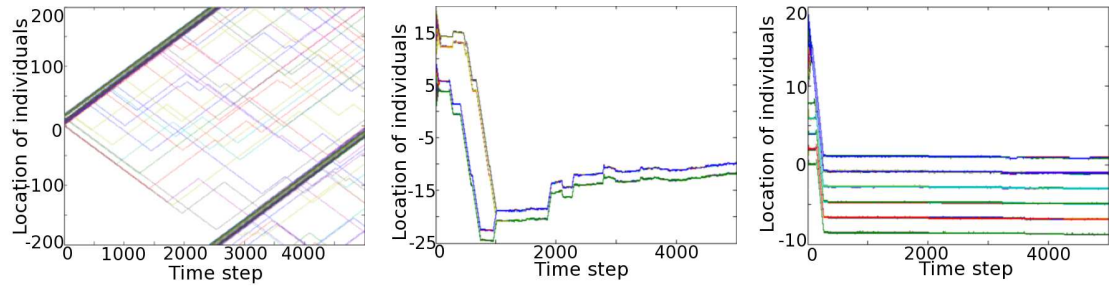

(a) (b) (c)

Figure 5.8: Aggregation patterns for varying values of m_a in the Eftimie-Kolpas hybrid submodel M1 with interaction kernels. (a) $m_a = 0.$; (b) $m_a = 1$; (c) $m_a = 4$. In (a), where there is no attraction, animals form a traveling pulse. This figure shows that a larger attraction zone decreases the likelihood of the group to be in the mobile phase ((b),(c)). Parameters used for both figures: $\tilde{q}_a = 10, n = 100, p = 0.001, m_r = 1, m_{al} = 1$.

The next aspect to investigate is how the animals' behavior would vary according to the size of the alignment zone, m_{al}. Figure 5.9(a) shows that for a small alignment zone, animals remain stationary. As the size of the alignment zone is increased, the group first transitions from stationary into semi-zig-zag pulses, and then from semi-zig-zag into zig-zag pulses (see Figures 5.9(b) and 5.9(c)). It is noteworthy that even when $m_{al} = 5.9$, the animals do not form traveling pulses. This is due to the fact that the attraction zone used is too large for a traveling pulse to be formed, a phenomenon observed in Figure 5.8. Hence, when the attraction zone is reduced, the group forms a single traveling pulse (see Figure 5.9(d)).

Finally, we explore the effects of varying the size of the repulsion zone, m_r. With a small repulsion zone, animals are mobile. When the repulsion zone is sufficiently large, the animals no longer travel (see Figure 5.10).

We summarize the results found from Figures 5.8, 5.9, and 5.10 in bifurcation diagrams (see Figure 5.11 and 5.12). These diagrams are not exact; rather, they are qualitative descriptions of how the behaviors change according to the sizes of the interaction zones. For example, Figure 5.11 shows how the aggregation behavior in the hybrid submodel M1 with interaction kernels changes according to the sizes of the alignment and attraction zones, which are given by m_{al} and m_a. For a large m_{al} and small m_a, traveling pulses are formed. For a large m_a, either zig-zag, semi-zig-zag, or stationary pulses are formed depending on the magnitude of m_{al}.

Having explored how each interaction affects the behavior of submodel M1, we now discuss the patterns produced by submodel M4. In submodel M4, we observe many of the same behaviors from submodel M1. However, for most parameter sets, there is a noticeably larger number of strayers and the pulses become more difficult to define. There are also a number of surprising and counterintuitive outcomes that we have not yet observed in previous implementations of the submodels. We discuss some of these below.

The first counterintuitive phenomenon is the transition from traveling pulses into a complete loss of aggregation behavior when the attraction zone is increased. For submodel M1, a larger attraction zone decreases the number of strayers (see Figure 5.8). For submodel M4, a sufficiently large attraction zone results in the animals not being able to aggregate in groups at all (see Figure 5.13).

Consistent with the scenario above, the animals lose their ability to form groups when the repulsion zone is decreased (see Figure 5.14). When m_r is sufficiently large, stationary pulses are formed. An increase in m_r results in a larger distance between each pulse. Figures 5.14(b) and 5.14(c) suggest that the animals prefer to form pulses that are spaced approximately $m_r + m_{al}$ apart, or where the attraction zone begins. The threshold value of m_r where the behavior transitions from stationary pulses to unorganized motion is approximately at 0.9. When m_r is near this threshold, animals can be in any one of the two patterns. The

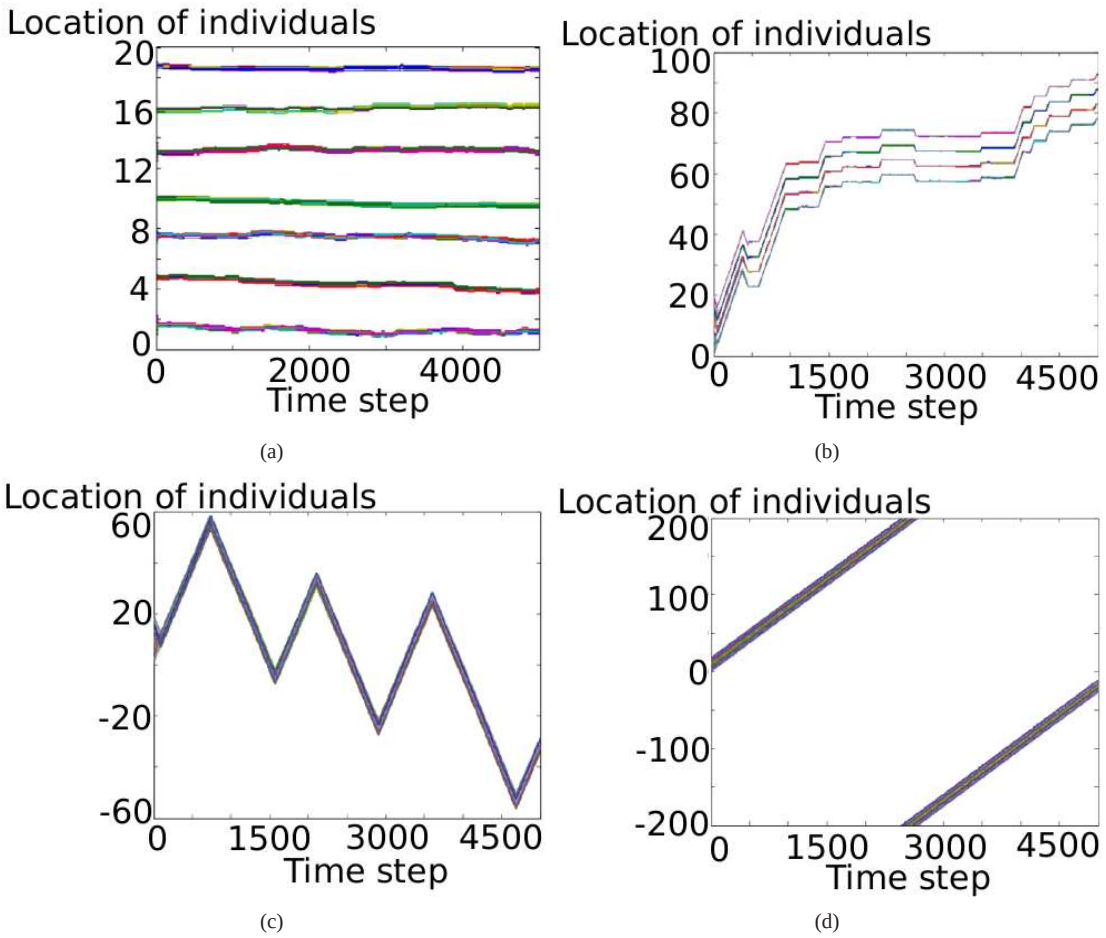

Figure 5.9: Aggregation patterns for varying values of m_{al} in the Eftimie-Kolpas hybrid submodel M1 with interaction kernels. (a) Stationary pulses with small alignment zone: $m_{al} = 0.1, m_a = 1$. (b) Semi-zig-zag pulses with intermediate alignment zone: $m_{al} = 4.9, m_a = 1$. (c) Zig-zag pulses with large alignment zone and large attraction zone: $m_{al} = 5.9, m_a = 1$. (d) Traveling pulses with large alignment zone and small attraction zone: $m_{al} = 5.9, m_a = 0.1$. This figure shows that a smaller alignment zone decreases the likelihood of the group to be in the mobile phase. Parameters used for all figures: $\tilde{q}_a = 10, n = 100, p = 0.001, m_r = 1$.

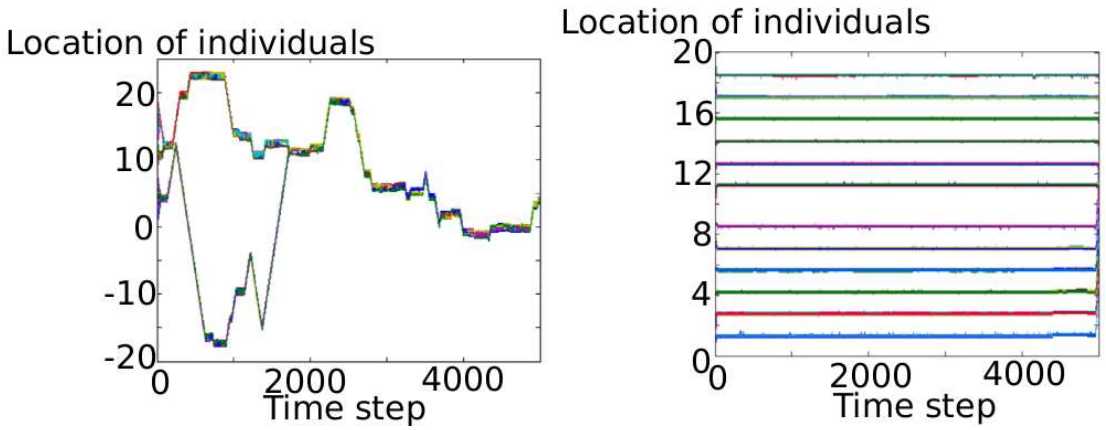

(a) (b)

Figure 5.10: Aggregation patterns for varying values of m_r in the Eftimie-Kolpas hybrid submodel M1 with interaction kernels. (a) Semi-zig-zag pulses with $m_r = 0.1$. (b) Stationary pulses with $m_r = 0.5$. This figure shows that a smaller repulsion zone increases the likelihood of the group to be in the mobile phase. Parameters used for both figures: $\tilde{q}_a = 10, n = 100, p = 0.001, m_r = 1, m_a = 1$.

equilibrium configuration most likely depends on the random initial conditions. Figures 5.13 and 5.14 give two criteria for forming cohesive groups in submodel M4: a small attraction zone and a large repulsion zone. If both requirements are not satisfied, the group does not exhibit any aggregation behavior. We would like to emphasize that to encourage group formation, we can either decrease the attraction zone or increase the repulsion zone. The effects from using a smaller attraction zone or a larger repulsion zone are similar since the two interactions are essentially opposites of each other. The alignment zone was also varied to explore its influence on the group behavior, but no noticeable changes in the patterns generated are found.

Having summarized the trends regarding the sizes of the attraction zones and the alignment zones, we discuss and summarize the surprising trends of submodel M4 (see Figure 5.15). From the results of submodel M1, we observe similar phenomena where large repulsion zones produce stationary pulses and small attraction zones produce traveling pulses. However, unlike submodel M1, submodel M4 cannot generate semi-zig-zag or zig-zag pulses. Instead, when either m_r or m_a is outside of the range where stationary and traveling pulses are found, animals simply do not aggregate. Given that the number of neighbors considered in submodel M4 are fewer compared to that in submodel M1, it is reasonable that the parameter space for pattern formation is smaller.

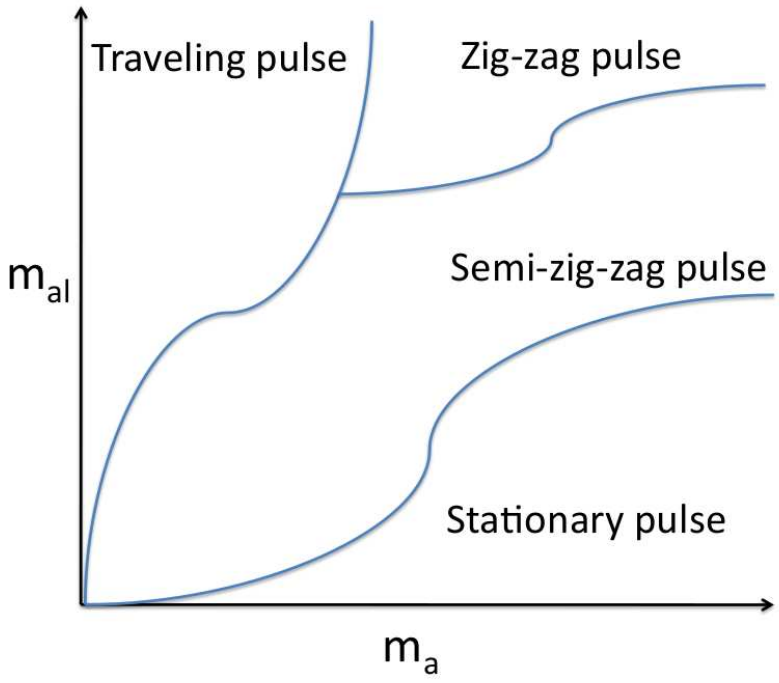

Figure 5.11: Two-parameter bifurcation diagram of the Eftimie-Kolpas hybrid submodel M1 with interaction kernels. The two parameters are m_{al} (size of the alignment zone) and m_a (size of the attraction zone). The group forms a traveling pulse if the alignment zone is large and the attraction zone is small. For intermediate sizes of alignment and attraction zones, the animals are in semi-zig-zag or zig-zag pulses. For a small alignment zone and large attraction zone, stationary pulses are generated.

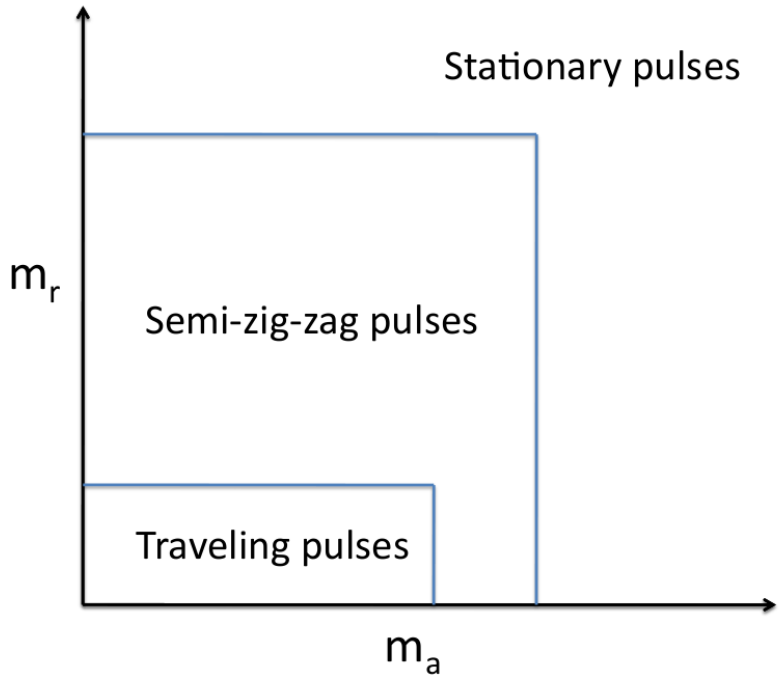

Figure 5.12: Two-parameter bifurcation diagram of the Eftimie-Kolpas hybrid submodel M1 with interaction kernels. The two parameters are m_r (size of the repulsion zone) and m_a (size of the attraction zone). The group forms a traveling pulse if both the attraction and repulsion zones are small. For intermediate sizes of repulsion and attraction zones, the animals travel in semi-zig-zag pulses. For large repulsion and attraction zones, stationary pulses are generated.

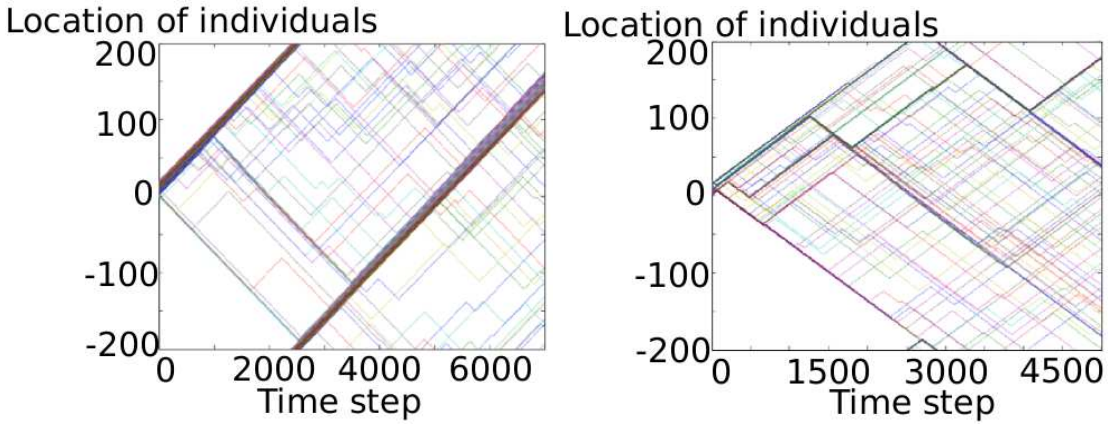

(a) No attraction. $m_a = 0$.

(b) Small attraction zone. $m_a = 1$.

Figure 5.13: Loss of aggregation behavior in the Eftimie-Kolpas hybrid submodel M4 with increased attraction zone. (a) $m_a = 0$; (b) $m_a = 1$. When there is no attraction (a), traveling pulses are formed. When a small attraction zone is added (b), the individuals lose the ability to form a cohesive pulse. Parameters used for both figures: $\tilde{q}_a = 30, n = 100, p = 0.001, m_r = 0.1, m_{al} = 1.9$.

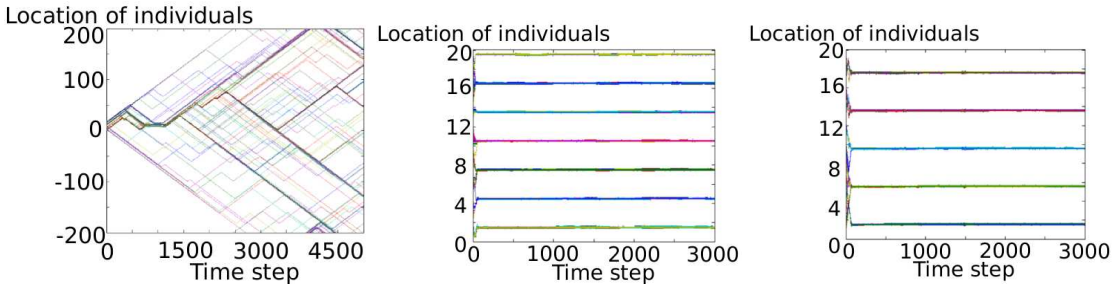

(a) Small repulsion zone. $m_r = 0.5$.

(b) Intermediate repulsion zone. $m_r = 2$.

(c) Large repulsion zone. $m_r = 3$.

Figure 5.14: Loss of aggregation behavior in the Eftimie-Kolpas hybrid submodel M4 with decreased repulsion zone. (a) $m_r = 0.5$; (b) $m_r = 2$; (c) $m_r = 3$. When the repulsion zone is too small (a), the individuals lose the ability to form a cohesive pulse. When the repulsion is sufficiently large ((b) and (c)), stationary pulses are formed. Parameters used for both figures: $\tilde{q}_a = 30, n = 100, p = 0.001, m_{al} = 1, m_a = 1$.

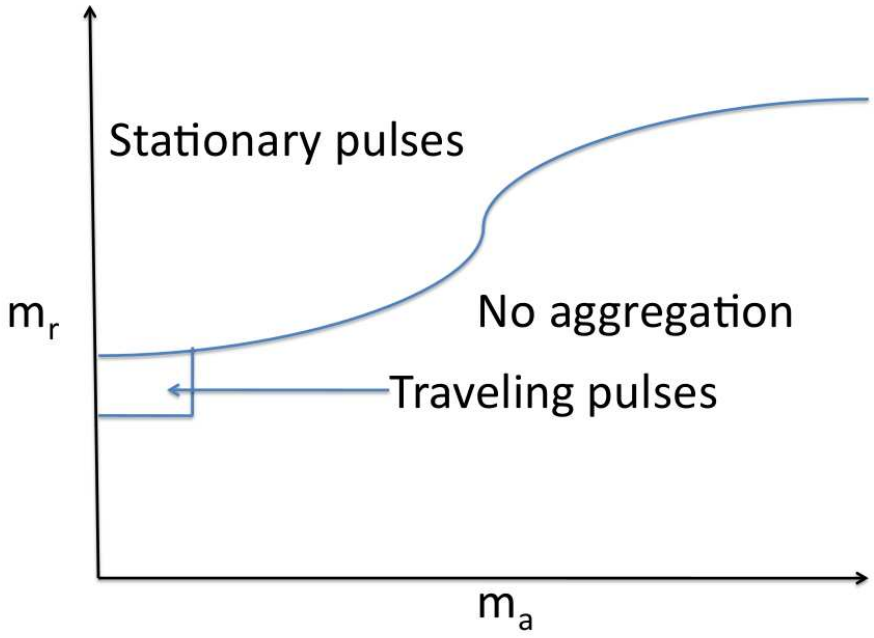

Figure 5.15: Two-parameter bifurcation diagram of the Eftimie-Kolpas hybrid submodel M4 with interaction kernels. The group forms a traveling pulse if the repulsion zone is in an intermediate range and the attraction zone is small. For intermediate sizes of repulsion and attraction zones, there is no aggregation behavior. For a large repulsion zone, stationary pulses are generated.

5.4 Discussion

In this chapter, we built a hybrid model based on the Kolpas and Eftimie models and investigated what types of behaviors the simulations would generate. We took the framework from the Kolpas framework and added direction-dependent communication. We investigated the hybrid model without and with interaction kernels. Because of the prioritization of repulsion, we find that in both versions of the Eftimie-Kolpas hybrid, the sizes of the interaction zones, instead of the parameter $\tilde{q}_a$, determine the behavior of the group. Also, in the hybrid model with interaction kernels, the reference individual must be able to receive signals from both sides to form patterns. This is a criterion that is not present in any other Lagrangian implementation in this project thus far.

The general behavior of the Eftimie-Kolpas hybrid depends on a relatively small set of parameters, which allows us to identify general trends easily. The results highlight the importance of the size of the interaction zones, as the group favors either being stationary or traveling with different values of $m_{r,al,a}$. The results establish that a large repulsion zone encourages the group to be stationary (see Figures 5.10 and 5.14), a large alignment zone increases the likelihood of the group to be in the mobile phase (see Figure 5.9), and a large attraction zone maintains the integrity of the group and keeps them in stationary pulses (see Figure 5.8). This is contradictory to what has been found by Schonfisch ([27]). The results from the cellular automata simulations in [27] show that while alignment alone can influence the animals so that they are traveling in one direction uniformly, no groups can be formed if attraction is not added. On the other hand, the Eftimie-Kolpas hybrid shows that alignment alone can produce traveling pulses, but an increase in the attraction, either by changing $\tilde{q}_a$ or m_a, results in the disappearance of this mobile behavior with fewer strayers (see Figures 5.8 and 5.4). This result is not surprising for the hybrid model since a stronger attraction means that animals attempt to minimize the number of strayers, which does not require for the animals to be traveling. Moreover, many of the traveling pulses produced from the rules of the Eftimie-Kolpas hybrid contain strayers, which explains why animals choose to remain stationary to preserve the population within the pulse when attraction is large. The optimal distance between each stationary pulse is determined by where the attraction zone begins. Submodel M1 produces the most patterns, including stationary, semi-zig-zag, zig-zag, and traveling pulses. This is most likely due to the fact that individuals in submodel M1 detect more neighbors than any other submodels displayed in Figure 2.1.

The Eftimie-Kolpas hybrid has produced many interesting results, some of which echo the findings from the Lagrangian version of the Eftimie model. For example, a non-uniform interaction kernel is required for the animals to exhibit interesting behaviors like zig-zag pulses. This discovery is encouraging because it

suggests that animals may, in fact, require such a strategy to form the interesting patterns that we observe in nature.

Chapter 6

Conclusion

6.1 Introduction

In this thesis, we explored direction-dependent communication mechanisms introduced by Eftimie *et al.* ([9], [10], [11]) in the context of Lagrangian approaches to modeling animal movement. The models share the common trait that individuals receive communication signals from neighbors in repulsion, alignment, and attraction zones. We explored two implementations: the individuals in the first implementation consider the signals in no preferential order, while the individuals in the second one prioritize repulsion over alignment and attraction signals. In addition, we investigated an ODE movement model with direction-dependent communication mechanisms, which is an intermediate between the Lagrangian models and the Eftimie PDE model.

One of our goals with animal movement modeling is to find the factors that determine what, if any, patterns can be formed with the Lagrangian and ODE versions of the Eftimie model. For these simulations, we assume that no communication signal is prioritized. With the Lagrangian models, we had the choice of using different interaction kernels to vary the signal strength, depending on the distance between the neighbor and the reference individual. Since the individual-based model was to be as similar to the Eftimie PDE model as possible, we chose to work with triangular and cut-off Gaussian kernels, which share many similarities with the original Gaussian kernels used by Eftimie *et al.* We also examined how different weights of signal strengths can affect the patterns formed in the Lagrangian models. Using different parameter sets, we were able to generate many of the patterns that Eftimie *et al.* found with the PDE model. Since the incorporation of direction-dependent communication mechanisms in the PDE and Lagrangian models generated such exciting results, we added the same communication rules in an ODE model. Here, we only used the Gaussian cut-off kernels in our simulations. Compared to the Lagrangian implementations, the

ODE model generated more patterns found by the Eftimie PDE model. This is due to the fact that the ODE model is a closer translation of the PDE model.

Finally, we introduced a hybrid model that incorporates the Eftimie model's direction-dependent communication rules in the Kolpas model, where repulsion is prioritized. Since repulsion is the only signal considered whenever it is present, we can only vary the relative weighting between alignment and attraction when there is no repulsion. As expected, a shift in this weighting has less of an influence when compared to the Eftimie ODE and Lagrangian models. Therefore, for the hybrid model, we focus on how the sizes of the interaction zones impact the behavior. The results show that alignment is very important for animals to form traveling pulses, which echoes the findings of the original Kolpas model.

The results of this thesis confirm that many of the patterns found with the Eftimie PDE formulation can be generated with a Lagrangian and ODE model. These include breathers, traveling breathers, stationary and traveling pulses, traveling trains, and zig-zag pulses. Some patterns, like the breathers and traveling breathers, have never been produced by any previous Lagrangian formulations. An alternating series of traveling and stationary pulses represents a group of animals migrating in a consistent direction and taking breaks in between.

In general, patterns generated with the models are anaglous to patterns observed for real groups of animals as they interact with their surroundings. In fact, aggregating in groups offers many advantages. For example, many types of fish, including guppies and pelagic fish, travel in schools for anti-predatory purposes, as the per-capita predation risk is assumed to decrease according to the group size ([19]). Therefore, being able to aggregate in traveling trains and pulses is an important survival skill. An alternating series of traveling and stationary pulses represents a group of animals migrating in a consistent direction and taking breaks in between. Depending on the situation, the group may be more or less densely packed. For instance, the groups may compress depending on whether vessels are passing above them ([13]). In this case, the fish are in the arrangement of a breather while the group expands and contracts continuously. In this formation, those at the boundary may deviate momentarily before returning to the group. Birds have also been known to display this type of behavior ([8]). Zig-zag patterns, which have been found in the Lagrangian, ODE, and Kolpas-Eftimie-hybrid models, are a part of the protean phenomena, where animals show unexpected movement and behavior so the predator cannot predict the prey's location ([15]). Buchanan *et al*. describe how dunlins escape predation from the merlins by rapidly switching orientation as an entire group ([3]). These biological examples highlight how important it is for animals to be able to aggregate and exhibit different patterns to adapt to the environment.

In the following section, we compare specific results from the Eulerian and Lagrangian formulations.

Finally, we discuss the implications and future work in Section 6.3.

6.2 Results from the Eulerian, ODE, and Lagrangian Formulations

Based on the interaction rules established by the Eftimie model ([9], [10], [11]), we simulated animal movement with both ODE and Lagrangian models. Each formulation has produced a different range of results. The Lagrangian models have produced biased and unbiased zig-zag pulses, breathers, traveling trains, and stationary and traveling pulses. Except for zig-zag pulses, the ODE model has generated all of the patterns exhibited by the Lagrangian models. In addition, it can generate the traveling breather, which could not be found with the individual-based simulations. This prompts us to ask when we should apply each model. In particular, we should consider the specific situations where these aggregation patterns are displayed in nature.

The Lagrangian formulation models the process where each animal senses its neighbors, decides whether or not to turn, and moves along the domain. There are several advantages that the Lagrangian approach has compared to the Eulerian one. First, instead of being able to receive signals from those who are infinitely far away, animals cannot sense their neighbors if they are not within a defined area. Second, by avoiding the use of any Taylor series to derive a PDE system, nonlinear interactions are included. Third, we factored in stochastic effects with the use of a uniformly generated random variable to decide if an animal changes direction.

In Chapter 3, we thoroughly explored the Lagrangian implementation of Eftimie's PDE model with three different interaction kernels: the uniform, triangular, and cut-off Gaussian kernels. With a uniform kernel, only stationary and traveling pulses were found. The pattern range using triangular and cut-off Gaussian kernels is much larger. By varying $q_{r,al,a}$, weights of the repulsion, alignment, and attraction signals, we found breathers, traveling, stationary, and zig-zag pulses, thus largely reproducing the results obtained with Eftimie's PDE model. We note that the groups generated by the Lagrangian formulation show a significant number of strayers, which is not the case for those generated by the Eulerian formulation. This emphasizes that stochasticity plays an important role in the individual-based formulations.

In Chapter 5, we further explored the role of direction-dependent communication mechanism in another Lagrangian model, namely the Kolpas model. In the resulting Eftimie-Kolpas hybrid, repulsion is prioritized over alignment and attraction. We generated patterns with and without interaction kernels using the hybrid model. The main parameters that we varied are the sizes of the interaction zones. A general trend that we have discovered from these simulations is that attraction plays a central role in maintaining the integrity

of the group, while alignment is crucial in forming traveling pulses. When a cut-off Gaussian interaction kernel is used, reference individuals must observe neighbors from both sides to lower the number of strayers and preserve the aggregation behavior. Moreover, the hybrid model has led us to discover interesting links between the interaction zones and the aggregation pattern. In general, a large attraction zone encourages animals to form groups, while a large repulsion zone has the opposite effect of increasing the number of strayers from groups. With a large alignment zone, animals are more likely to be traveling. We found many patterns with the hybrid model, including stationary, semi-zig-zag, zig-zag, and traveling pulses.

While the results are biologically relevant for both the hybrid and the Lagrangian Eftimie models, one important limitation they share is that animals are restricted to moving only at certain times. This is not the case for most organisms, which leads us to look for another method to model animal movement in Chapter 4. The ODE formulation using assumptions from the Eftimie model removes this restriction by making time continuous and keeping space discrete. We can view the spatial step as a representation of the species' average stride length. Similar to the Lagrangian model, the cut-off Gaussian interaction kernels have compact support, defining a specific neighborhood where neighbors can exert an influence on the reference individual's movement. Using different values of $q_{r,al,a}$, this model has produced traveling and stationary breathers and pulses along with traveling trains. Both traveling and stationary breathers and pulses are common in nature. Traveling trains are simply when an entire group travels one direction in several files.

The PDE formulation with only continuous variables has produced the largest range of aggregation patterns. Continuous space is suitable for describing simple animals like fish and snakes who do not move forward in steps. Those unique to the PDE model are feathers and ripples. When animals are in the feather formation, they are stationary, but individuals at the boundary are lost slowly, traveling away from the group until they return to the group due to the periodic boundary conditions. This may not be biologically realistic, as departing from the main group is usually not beneficial for group animals. In fact, it is shown that many predators tend to attack those who stray far away from the group ([3]). The biggest benefit of using the PDE formulation is that it is effective in determining the effect of each parameter on pattern formation, using analytical results from bifurcation theory and dispersion relations.

Having fully exploited the use of continuous and discrete variables in the Eftimie animal movement model, we now have an improved understanding of the model, and obtained further insight into the effect of such direction-dependent communication mechanisms. In general, the inclusion of direction-dependent communication mechanisms significantly enriches model behavior in the sense that a broader range of aggregation patterns can be obtained. Many of the simulated patterns can be found in nature. This underscores the likely importance of direction-dependent communication mechanisms.

6.3 Future Work

In this thesis, we continued the work of Eftimie *et al*. in modeling animal movement with direction-dependent communication mechanisms. Similar to its Eulerian predecessor, the ODE and Lagrangian models have succeeded in producing a wide range of behaviors. This is, however, only a small part in fully understanding how the individual social interactions may influence the global group structure. In this section, we will discuss some unanswered questions and possible future research directions.

In Chapter 3, we translated the Eftimie model into a discrete-time Lagrangian model. While the main features of the original model have been preserved, others needed to be altered to accommodate the discretization and change in modeling perspective. One of the features that we modified is the interaction kernel, which has been thoroughly introduced in Sections 3.7 and 3.8. The main modification from the kernels used in the original Eftimie model is that the interaction zones are now bounded. Compared to the original kernels, the modified kernels can be argued to be a more realistic representation of what is found in nature because animals cannot sense neighbors from infinitely far away. However, the cut-off of the originally infinite interaction kernel domain may have altered the numerical results of the Lagrangian formulation, and perhaps explain why we found a smaller range of patterns compared to the Eulerian model. More work is needed to confirm this. Second, the representation of discrete interaction kernels is not limited to the two that we have chosen for this project, and there are many more that we could explore. Currently, the neighbors who are adjacent to the reference individual exert the smallest repulsion force. This is not biologically realistic, providing a motivation to explore interaction kernels which are not similar to the Gaussian kernel. Another question that remains to be answered is how exactly do the nonlinear interactions and stochastic effects incorporated in the Lagrangian implementation affect our results?

In Chapter 4, we modeled how animals move on a gridline in continuous time. Again, we followed the basic principles from the Eftimie model with the exception of space discretization. Here, we see a larger range of results produced from one implementation compared to both the Lagrangian implementations with two different interaction kernels. This is expected because this formulation incorporates less changes into the system by avoiding time discretization. However, we should note that the ODE formulation is no longer a Lagrangian implementation because the model tracks the number of animals at each location instead of the individuals themselves. An interesting variation to consider for future research is if a model in discrete time and continuous space is possible. For such a system, it would be possible to track each individual in continuous space.

In Chapter 5, we added components of the Eftimie model into the Kolpas Lagrangian model, which has

a similar framework to the Lagrangian model in this project. We assume that the communication between animals is direction-dependent and repulsion is the most important social interaction. Using the five different submodels introduced in Figure 2.1, we are able to find stationary, semi-zig-zag, zig-zag, and traveling pulses. Interestingly, submodels 3 and 5 are not able to produce any aggregation patterns at all when cut-off Gaussian interaction kernels are added. This suggests that when repulsion is prioritized, the ability to receive signals from all directions is important in forming groups. Moreover, the results reflect the general trend that a large alignment zone encourages the animals to travel while a large attraction zone helps animals aggregate in groups. For the Kolpas model, there is a statistical measure that helps quantify the effects that the size of the alignment zone has on the model behavior. It would be interesting to introduce a similar measure to the hybrid model to define the influence of each interaction quantitatively, as we now only have a qualitative description for the impact of each parameter.

Finally, there are more possibilities in how we choose the communication mechanisms. Eftimie suggests extending the model to higher dimensions, which is a component not explored in this project ([8]). Modeling in higher dimensions raises complications in determining which neighbors send communication signals according to their orientation and location. On the other hand, this is a very important step because animals like fish that exhibit behavior generated by the Eftimie model move in 3-D space. Also, we have not exhausted the possibilities for the rules dictating the direction-wise communication mechanism. Having extended the model to higher dimensions, we are no longer limited to only differentiating the neighbors at the front or the back. In fact, in the example of fish, many can only see on the side but not at the front because of the position of their eyes. Therefore, we may incorporate more factors into how signals from the side may be stronger than the signals from the front and back. There are many areas that remain to be explored on this topic, and the consideration of additional factors will allow us to find more patterns formed by animals in different situations.

Bibliography

[1] M. Adioui, J.P. Treuil, and O. Arino. Alignment in a fish school: a mixed lagrangian-eulerian approach. *Ecol. Model.*, 167:19–32, 2003.

[2] E. Ben-Jacob, I. Cohen, and H. Levine. Cooperative self-organization of microorganisms. *Adv Phys*, 2000.

[3] J. Buchanan, C. Schnick, L. Brennan, and S. Herman. Merlin predation on wintering dunlins: Hunting success and dunlin escape tatctics. *Wilson Bull.*, 1988.

[4] I.D. Couzin, J. Krause, R. James, G.D. Ruxton, and N.R. Franks. Collective memory and spatial sorting in animal groups. *J. Theor. Biol.*, 218:1–11, 2002.

[5] C.Topaz, A. Bertozzi, and M. Lewis. A nonlocal continuum model for biological aggregation. *Bull. Math. Biol.*, 2006.

[6] F. Cucker and S. Smale. Emergent behavior in flocks. *IEEE Trans. Biomed. Eng.*, 52(5), 2007.

[7] L. Edelstein-Keshet, J. Watmough, and D. Grunbaum. Do travelling band solutions describe cohesive swarms? an investigation for migratory locusts. *J. Math. Biol.*, 36(6):515–549, 1998.

[8] R. Eftimie. *Modeling Group Formation and Activity Patterns in Self-Organizing Communities of Organisms*. PhD thesis, University of Alberta, 2008.

[9] R. Eftimie, G. de Vries, and M.A. Lewis. Complex spatial group patterns result from different animal communication mechanisms. *P. Natl. Acad. Sci.*, 104:6974–6979, 2007.

[10] R. Eftimie, G. de Vries, and M.A. Lewis. Weakly nonlinear analysis of a hyperbolic model for animal group formation. *J. Math. Biol.*, 59:37–74, 2007.

[11] R. Eftimie, G. de Vries, M.A. Lewis, and F. Lutscher. Modeling group formation and activity patterns in self-organizing collectives of individuals. *Bull. Math. Biol.*, 69:1537–1565, 2007.

[12] G. B. Ermentrout and L. Edelstein-Keshet. Cellular automata approaches to biological modeling. *J. Theor. Biol.*, 160:97–133, 1993.

[13] P. Freon, F. Gerlotto, and M. Soria. Changes in school structure according to external stimuli: description and influence on accoustic assessment. *Fish. Res.*, 1992.

[14] S. Gueron, S. Levin, and D. Rubenstein. The dynamics of herds: from individuals to aggregations. *J. Theor. Biol.*, 182:85–98, 1996.

[15] D.A. Humphries and P.M. Driver. Protean defence by prey animals. *Oecologia*, 1970.

[16] A. Huth and C. Wissel. The simulation of the movement of fish schools. *J. Theor. Biol.*, 156:365–385, 1992.

[17] A. Huth and C. Wissel. Analysis of the behavior and the structure of fish schools by means of computer simulations. *Comments Theor. Biol.*, 1993.

[18] A. Kolpas, J. Moehlis, and I. G. Kevrekidis. Coarse-grained analysis of stochasticity-induced switching between collective motion states. *P. Natl. Acad. Sci.*, 104(14):5931–5935, April 2007.

[19] J. Krause and J. Godin. Predator preferences of attacking particular prey group sizes: consequences for predator hunting success and prey predation risk. *Anim. Behav.*, 1995.

[20] H. Levine and W. Rappel. Self-organization in systems of self-propelled particles. *Phys. Rev. E*, 63(1), 2000.

[21] R. Lukeman, Y.X. Li, and L. Edelstein-Keshet. A conceptual model for milling formations in biological aggregates. *Bull. Math. Biol.*, 2008.

[22] V. Mirabet, P. Auger, and C. Lett. Spatial structures in simulations of animal grouping. *Ecol. Model.*, 2007.

[23] A. Mogilner and L. Edelstein-Keshet. A non-local model for a swarm. *J. Math. Biol.*, 38:534–570, 1999.

[24] A. Okubo and S. Levin. *Diffusion and Ecological Problems: Modern Perspectives*. Springer-Verlag New York, Inc., 2001.

[25] H. Reuter and B. Breckling. Self-organization of fish schools: an object-oriented model. *Ecol. Model.*, 1994.

[26] W. Romey. Individual differences make a difference in the trajectories of simulated schools of fish. *Ecol. Model.*, 1996.

[27] B. Schönfisch. Simple individual based models of movement, alignment and schooling behavior. *Future Gener Comp Sy*, 2001.

[28] P. Turchin. *Quantitative Analysis of Movement*. Sinauer Associates, Inc., 1998.

[29] K. Warburton and J. Lazarus. Tendency-distance models of social cohesion in animal groups. *J. Theor. Biol.*, 150:473–488, 1991.

[30] Y.X.Li, R. Lukeman, and L. Edelstein-Keshet. Minimal mechanisms for school formation in self-propelled particles. *Physica D*, 237(5), 2008.